Pharmacokinetic and Pharmacodynamic Properties of Cationic Liposomal Delivery of the Immunomodulatory Agent R848 to the Mouse Peritoneal Cavity for the Treatment of Advanced Peritoneal Cancer

by

Griffin William Pauli

BScH., Queen's University, 2018

A THESIS SUBMITTED IN PARTIAL FULFILLMENT OF
THE REQUIREMENTS FOR THE DEGREE OF

MASTER OF SCIENCE

in

THE FACULTY OF GRADUATE AND POSTDOCTORAL STUDIES

(Pharmaceutical Sciences)

THE UNIVERSITY OF BRITISH COLUMBIA
(Vancouver)

August 2020

The following individuals certify that they have read, and recommend to the Faculty of Graduate and Postdoctoral Studies for acceptance, the thesis entitled:

Pharmacokinetic and pharmacodynamic properties of cationic liposomal delivery of the immunomodulatory agent R848 to the mouse peritoneal cavity for the treatment of advanced peritoneal cancer

submitted by Griffin Pauli in partial fulfillment of the requirements for

the degree of Master of Science

in Pharmaceutical Sciences

Examining Committee:

Dr. Shyh-Dar Li, Pharmaceutical Sciences
Supervisor

Dr. Mark Harrison, Pharmaceutical Sciences
Supervisory Committee Member

Dr. Judy Wong, Pharmaceutical Sciences
Supervisory Committee Member

Dr. Harvey Wong, Pharmaceutical Sciences
Additional Examiner

Additional Supervisory Committee Members:

Dr. Karla Williams, Pharmaceutical Sciences
Supervisory Committee Member

Dr. Gregor Reid, BC Children's Hospital
External Committee Member

Abstract

Peritoneal cancer, defined as malignancies on the lining of the abdominal viscera, often originates from metastatic lesions in the ovaries, stomach and colon. The diffuse spreading of this cancer in the abdominal cavity makes it difficult to treat and causes relatively high recurrence rates. Currently, peritoneal cancer is treated by cytoreductive surgery and locoregional chemotherapeutic regimes. This procedure is associated with high morbidity and mortality, while not being sufficiently effective in diminishing recurrence rates. We hypothesized that peritoneal cancer treatment could benefit from an immunotherapeutic approach to reduce recurrence via generation of an anti-tumour immune response and modulation of the tumour microenvironment. To address this, we developed a liposome-based delivery system for the immune boosting agent Resiquimod (R848). We found that the liposomes incorporated with a positively charged lipid 1,2-stearoyl-3-trimethylammonium-propane (DSTAP) delivered by intraperitoneal (IP) injection increased peritoneal retention of R848 while minimizing its systemic absorption. Specifically, we observed that the peritoneal area under the curve concentration of R848 was 14 times greater when in the DSTAP-liposomes relative to the free drug formulation. Within 1 h post IP injection, ~60% of monocytes and macrophages, ~10% dendritic cells and ~8% natural killer (NK) cells in the peritoneal fluid were found to contain the liposomes. DSTAP-R848 significantly upregulated the production of TNF-α (2-fold), IL-6 (4-fold) and IFN-α (10-fold) mRNA relative to PBS control, leading to significantly reduced tumour progression in an IP metastasis model of CT-26 colorectal cancer in mice. Free R848 was ineffective in inducing the immune promoting cytokines nor antitumour efficacy. We demonstrated that DSTAP-R848 increased the trafficking of innate immune cells, specifically NK cells, in the peritoneal cavity.

Lay Summary

Abdominal cancers are difficult to treat due to growth in a variety of tissues. Advancements in surgical techniques and chemotherapy have increased the survival of abdominal cancer patients, however, recurrence rates remain high. Immunotherapy, using one's immune system to combat cancer, could help prevent recurrence. Immunotherapy requires highly targeted treatments as non-specificity can cause severe toxicity. We formulated a positively charged lipid sphere (liposome) which encloses R848, an immune-boosting agent. The liposome formulation kept R848 inside the mouse abdomen and increased production of anti-tumour cytokines. We found that it could slow spread of aggressive colorectal cancer when administered with a chemotherapeutic drug. We discovered that our formulation increases the presence of Natural Killer cells in the abdomen. These cells serve to defend against transformed cells. We hope that this immune boosting drug could be an additional item in the surgeon’s toolbox when treating abdominal cancer.

Preface

This thesis is composed of one manuscript that will be submitted for publication. Details of the specific nature of the experiments and the scope of the thesis work were formulated in discussions between Dr. Shyh-dar Li, Suen Lee, Dr. Zhu Qin, Po Han Chao and myself. I received training and worked with Dr. Zhu Qin, Dr. Roland Böttger and Po Han Chao to complete the aims described in this thesis. Assistance with flow cytometry was given by Andy Johnson at UBC flow center. This thesis was written by me, under the guidance of Dr. Shyh-Dar Li.

Table of Contents

List of Tables

List of Figures

List of Abbreviations

APC	Antigen presenting cell
BD	Biodistribution
CD	Cluster of differentiation
Chol	Cholesterol
DC	Dendritic cell
DiI	1'-Dioctadecyl-3,3,3',3'-Tetramethylindocarbocyanine Perchlorate
DLS	Dynamic light scattering
DSPC	1,2-distearoyl-sn-glycero-3-phosphocholine
DSPG	1,2-Distearoyl-sn-glycero-3-phospho-rac-glycerol
DSTAP	1,2-stearoyl-3-trimethylammonium-propane
ELS	Electrophoretic Light Scattering
XELOX	Capecitabine, Oxaliplatin (chemotherapy cocktail)
FACS	Fluorescence-activated Cell Sorting
FOLFOX	Folinic Acid, Fluorouracil, Oxaliplatin (chemotherapy cocktail)
HIPEC	Hyperthermic Intraperitoneal Chemotherapy
IFN	Interferon
MDSC	Myeloid Derived Suppressor Cell
NK	Natural Killer
NKp46	Natural Killer cell maturation protein
OXA	Oxaliplatin
pAPC	Professional Antigen Presenting Cell
PC	Peritoneal cancer
PDI	Polydispersity Index
PDL-1	Programmed Death Ligand 1
PK	Pharmacokinetics
PPCa	Primary Peritoneal Cancer
PRR	Pattern Recognition Receptor
R848	Resiquimod
TAM	Tumour Associated Macrophage
TIME	Tumour Immune Microenvironment
UPLC	Ultra High-Performance Liquid Chromatography

Acknowledgments

The past two years have been such a profound learning experience and a period during which I did a significant amount of self-reflection. I am very grateful to the incredible lab mates, and now friends, I have made in the Faculty of Pharmaceutical Sciences for supporting me in every facet imaginable. My most sincere thanks go out to you all; Zhu Qin, Lukas Hohenwarter, Anne Nguyen, Roland Böttger, Nojoud Al Fayez, KK Viswanhan, and Po Han Chao. I would like to highlight a special thanks for Po Han, Zhu, and Roland for mentoring me and helping me refine my laboratory skills and scientific inquisition. I wish you only the best in what will certainly be amazing careers.

I need to also express a great thanks to friends outside the lab in my time with PharGS, PharmSci EDI among other committees. It was fantastic to be a part of something so vital to our Faculties ever-so-present sense of community. Thanks to Kate, Louis, Ariana, Jen and Hayley for their mentorship. Thanks to Karan for the coffee runs (and some fun nights with Lukas).

A thanks is overdue as well to technical staff: Andy at the UBC Flow Center for some heated conversations! Sarah Hulme of the modified barrier facility and Goubin at the UBC Center for High Throughput Genomics for his unbridled patience.

I owe a great deal of thanks as well to Dr. Thomas Massey for mentoring me in my undergraduate thesis and to Dr. Shyh-Dar Li for accepting me into this lab and being so available for help at all times during the day and night. I would also like to thank my parents Bruce and Lori and my “Vancouver parents” Uncle Mac and Aunt Sue for helping me immensely - could not have done it without you four! Lastly, I owe all of this to my partner who has been there and through all of this with me: Alexandra Sylvester. She has been with me at my worst and best and this thesis is dedicated to you.

Chapter 1: Introduction

1.1 Peritoneal Cancer and its Current Treatment

Peritoneal cancer (PC) describes malignancies in the serous mesothelial lining of the abdominal viscera, diaphragm and pelvis [1]. PC originates from spontaneous mutations in these epithelial cells (primary PC), or more commonly, from peritoneal-free cancer cells (PFCC), cells which have metastasized from distant tissues such as the ovaries, colon and stomach where they adhere to the peritoneal lining [2]. Until the late 1990s, PC was treated palliatively, or with surgical resection, and was accompanied by dismal survival rates wherein median survival ranged from 8-13 months [3,4]. However, recent advancements in surgical and perioperative chemotherapy approaches have increased 3- and 5- year recurrence free survival from 5.87% and 3.76% up to 20.40% and 17.05% respectively (P =0.001) [4,5]. The recently developed standard of care in the majority of PC includes cytoreductive surgery (CRS) and perioperative hyperthermic intraperitoneal chemotherapy (HIPEC) [2]. The goal of CRS is to resect all macroscopic lesions in the surgical field. Subsequently, locoregional application of chemotherapeutic regimes such as FOLFOX/XELOX is used to diminish microscopic malignancies and kill PFCC. Bathing the peritoneal lining and its enclosed contents with hyperthermic chemotherapeutics offers several advantages over CRS alone or CRS + systemic chemotherapy. The locoregional approach allows for a high drug concentration in the peritoneal compartment and minimal systemic distribution as the peritoneal lining is poorly perfused and the chemotherapeutic fluid is aspirated prior to the closing of the abdomen. This increases tumour penetration of the drug and reduces off-target toxicity. In addition, the direct application in the intraperitoneal (IP) compartment allows for high pressure hyperthermic (41-43^{o} C) infusion temperatures. This has been well documented both experimentally and clinically to increase cytotoxicity and tumour penetration and immune responses against solid tumours [3,6]. Indeed, Oxaliplatin (OXA), a component of FOLFOX/XELOX, has been shown to have potentiated antineoplastic effects when dosed at higher temperatures [3]. However, despite these major advancements in PC screening, quantification and management, treatment outcomes remain suboptimal. In addition, this procedure continues to be

associated with high morbidity and mortality and is thus often contradicted for those over 70 years of age [7]. Another major issue facing the management of PC is the high rate of recurrence observed with this disease – between 70 - 90% depending on the success of cytoreduction [8,9]. While the exact mechanisms behind the high recurrence rate have yet to be fully delineated, mounting evidence points to the involvement of multifocal malignant cell populations, limited tumour penetration of drugs, and highly drug resistant tumour populations [10]. To address the high recurrence rate, treatment of PC could benefit from the involvement of immune memory against transformed cells. This may more effectively clear the abdominal cavity and resist seeding of PFCC that could continue to invade the abdominal cavity. However, through a process of natural selection and random mutation, tumours cells that are detected by immunosurveillance are cleared, leaving only those that remain undetectable either through upregulation of inhibitory surface markers such as PD-1 and CTLA-4 or the secretion of cytokines that recruit immunosuppressive cells such as tumour associated macrophages and Treg cells . The sculpting of the tumour cells and their surrounding can lead to the formation of a Tumour Immune Microenvironment (TIME).

1.2 Immunomodulation of the Tumour Immune Microenvironment

1.2.1 The Tumour Immune Microenvironment (TIME)

The tumour immune microenvironment (TIME) is the composition of the local tumour microenvironment in addition to the immune cell profile. The microenvironment refers to the physiological factors including underdeveloped vasculature and lymphatic vessels, cycling hypoxia and upregulation of cancer-associated fibroblasts [11]. The immune aspect refers to the distinct immune cell profile of the tumour. This often includes an increase in immunosuppressive cells such as myeloid derived suppressor cells (MDSCs), tumour associated macrophages (TAMs) and T_{reg} cells [12]. The TIME of the peritoneum remains a largely understudied aspect of PC management. It is known that the tumour environment of PC is often heterogeneous, owing to the diverse sites of metastasis and the stem-cell like attributes present in many

PFCC [10]. Despite this, the PC TIME does share commonalities with TIME in other sites, such as cycling hypoxia, abnormal pH levels, and fibrosis. In addition to changes in anatomical and physiological features, the PC TIME also possess a unique immune environment characterized by infiltrating leukocytes and tertiary lymphoid structures [13].

1.2.2 Immune Aspect of the TIME

The TIME can be subdivided by the presence of immune cell infiltrate and cell surface expression into 3 classes; infiltrate excluded (I-E, highly immunosuppressed), infiltrate inflamed (I-I, some immunosurveillance) and infiltrate tertiary lymphoid structure supported (I-TLS, highly immunopotentiated). Epithelial cell tumours such as colorectal carcinoma, melanoma and pancreatic duct adenocarcinoma are often associated with an immunosuppressed (I-E) profile, wherein there is downregulation of inflammatory cytokines such as Type 1 Interferons (IFNs alpha, beta), Tumour Necrosis Factor Alpha (TNF-α), Interleukin (IL)-2, IL-6, IL-17. In addition, there is a corresponding change to the immune cell profile of the tumour. The I-E tumour has higher levels of cancer-associated fibroblasts (CAFs), M2-like macrophages, myeloid-derived suppressor cells (MDSCs), regulatory T cells (T_{reg}) [14,15]. These tumours also frequently have poor infiltration of cytotoxic lymphocytes (CTLs) such as CD8+ T cells and Natural Killer (NK) cells in the tumour core. Lastly, the I-E TIME also has increased cell surface expression of inhibitory ligands such as PDL1-2 and CTLA-4 [16]. In contrast, I-I and I-TLS tumours are observed to have increased penetration of CTLs, the presence of M1-like macrophages and other professional antigen presenting cells such as dendritic cells (DCs). There is also an increase in inflammatory cytokines and chemokines and a downregulation of inhibitory cell surface ligands. Overall, this inflammatory environment correlates to a better prognosis for response to common immunotherapies such as immune checkpoint blockade (ICBs) and tumour clearance due to the fact there is an increased presence of CTLs and downregulation of inhibitory cell surface markers [17].

The process that generates this immunosuppressive cell and surface marker profile is known as "immunoediting". In this process, tumours will undergo three stages of editing referred to as elimination, equilibrium and escape. In the first phase "elimination", the immune system will systematically destroy any transformed cells that are recognized as transformed. However, this form of natural selection will lead to tumour cells that are not detected, either due to downregulation of non-self antigen or upregulation of immunoinhibitory markers. These undetected cells can proliferate in the "escape" phase where tumours growth begins outpacing immune surveillance and lead to greater tumour load [18]. Overall, this process can sequentially sculpt the TIME to favour the expression of these inhibitory markers, thus diminishing the host immune response against the tumour. The goal of immune modulating agents is to shift this balance and reverse the immunoediting process to favour the detection and destruction of tumour cells.

1.2.3 Modulation of the TIME

The modulation of the TIME has seen a great deal of attention in the field of immuno-oncology. Specifically, modulation of the TIME involves a change in overall phenotype of the tumour and its environment. This is often characterized by a change in cellular infiltrates, immune cell surface marker expression, and local cytokine expression [19]. A goal of immune modulation is to minimize the presence of inhibitory cell surface markers (such as PDL-1/2 and CTLA-4) and increase the penetration of tumour infiltrating lymphocytes that can produce anti-tumour immunity or respond to immune checkpoint blockade (ICB) therapy. Specifically, immune modulation attempts to increase the presence of CD8+T cells, NK cells and M1-like macrophages and lower percentages of CD4+ FOX3P+ T cells (T_{reg}) Cells, M2-like macrophages, MDSCs, TAMs and CAFs. This reversal has been consistently shown to improve outcomes in animal and some human studies [8,20–22]. In addition, more macroscopic changes such as vascular remodelling and lymphatic structure morphology can occur in the remodelling of the TIME such as the development of lymph aggregates that can further boost tumour immunosurveillance and the reduction of angiogenesis via IFN-α secretion. [15,23,24].

1.2.4 Approaches for TIME Modulation and R848: An Imidazoquinolinone Immunomodulatory Agent

To accomplish TIME plasticity, recent research has implemented a four major classes of tactics such as 1) antibodies against immunosuppressive cells and their respective surface markers, i.e. immune checkpoint blockade (ICB). ICB has shown promise through antibody mediated blocking of PD-1/PDL-1 and CTLA-4, thus preventing T cell exhaustion and increasing T cell priming/activation [25]. 2) Cancer vaccines are also being investigated as a means for modulating the immune interaction with the tumour. By purifying TAA's this method hopes to boost antigen uptake and presentation to CTL's. 3) T cell engagement therapies are another class of modulating TIME which work by increasing the efficient of the synapse between a T cell, APC and tumour cell to boost antitumour immunity. 4)Finally there are the broadly acting immune boosting agents. This project focuses on this fourth class of TIME modulators, immune boosting agents. Immune boosting agents broadly upregulate aspects of the innate and humoral immune responses to reverse the immune suppressed tumour [26]. There are several targets for immune boosting agents that act through pattern recognition receptors (PRRs). This includes nucleotide-binding oligomerization domain (NOD)-like receptors (NLR), C-type lectin (CLR), RIG-I–like receptors (RLRs), cytosolic DNA sensors, stimulator of interferon genes (STING) and Toll-Like Receptors (TLRs). Among these immune activating agents, those acting on TLRs, a group of pattern recognition receptor, are the most studied. There are 13 TLRs expressed in mice and 10 TLRs expressed in humans, recognizing a variety of ligands. TLRs are expressed in a variety of immune cells including monocytes, macrophages, dendritic cells, B cells, T cells and NK cells. The TLRs are localized to the cell surface or in endosomes inside the cell. TLRs 1, 2, 4, 5, and 6 are localized to the plasma membrane and face the extracellular environment. TLRs 3, 7, 8, and 9 are localized to endosomes and lysosomes [27]. As the TLRs are involved in the initiation of and linkage of the innate and adaptive immune response, they can be leveraged to promote TIME modulation. To accomplish TIME modulation using TLR agonists, research has been focused on the delivery of TLR agonists to the TIME. The TLRs function to recognize damage/pathogen associated molecular patterns (D/PAMPs) found on bacteria or released from dying

cells. The TLRs recognize distinct structures and signal through multiple pathways[28]. In regard to agonists, TLR 1 and TLR 2 bind lipoproteins, TLR 3 binds (double stranded) dsDNA, TLR 4 which binds lipopolysaccharide (LPS), TLR 5 binds bacterial motifs, TLR 6 lipopeptides, TLR 7 and TLR 8 bind single stranded RNA (ssRNA) and synthetic purine derivatives, such as R848. TLR 9 binds CpG motifs.[28,29].

R848 (Resiquimod) belongs to a family of imidazoquinoline analogs that also includes Imiquimod, Dactolisib, Gardiquimod and Sumanirole (**Figure 1)** [30]. These derivatives share a common tricyclic ring structure and often have antiviral and anti-tumour properties [30–32]. After diffusing through the cell bilayer due to the hydrophobic nature of R848 (logP 2.24), R848 initiates its effects through binding of the TLR 7 and TLR 8 found in the endosomal compartment of a variety of innate immune cells including phagocytes [32]. TLR 7 and TLR 8 exists in a dimer[33]. Upon binding of an agonist by TLR 7/8 a conformational change occurs and recruits the adaptor protein myeloid differentiation primary response 88 (MyD88). MyD88 coordinates the recruitment of a variety of downstream signalling proteins including IRAK1,2,4, TAK1 and MAPKs. These proteins further recruit signalling molecules that culminate with recruitment of three promoters NFkB, IRF3/7 and AP-1 that begin binding DNA and increasing gene expression of cytokines IFN-α , IL-6, IL-12 and TNF-α , seen in **Figure 2** below [32]. R848 has been demonstrated to be the most potent of the imidazoquinoline analogs in regard to its ability to upregulate transcription of TNF-α and IL-6, two inflammatory gene products critical to inducing the innate and humoral immune response [31]. A complete list of cytokines that are secreted in response to R848 stimulation is shown below in **Table 1** and the important cytokines for this study are highlighted. There has been interest in using R848 to modulate the TIME due to its potent immunostimulatory effects. Through upregulation of inflammatory cytokines such as TNF-α, IFN-α and IL-6, and stimulatory ligands CD80 and 86 on DCs, R848 can increase the activation of T cells and NK cells [34]. R848 can also increase the resistance of T cells to exhaustion by MDSCs and reverse the differentiation of

immunosuppressive T_{reg} cells [35]. Moreover, R848 can decrease immunosuppression by inducing changes in innate immune cells of the tumour. Indeed, R848 has been shown to influence the TIME *in vivo*. A 2018 study by Rodell et al. [36] found that R848 could change the polarization of M2-like macrophages to M1-macrophages, indicating a reversal of an immunosuppressive TIME in a murine model. Moreover, a 2019 study by Mullins et al. [37] discovered that the TLR 7 and TLR 8 agonist MEDI9197, an analog to R848, could induce a T_h1 response in the tumour after intratumoural injection. In addition, when this analog was injected in combination with ICB agents, survival was prolonged. Lastly, in 2020, Chen et al. [38] further refined the R848 TIME modulation approach by using a near infrared (NI) responsive polymer loaded with R848 to boost anti-tumour immunity via an *in situ* cancer vaccine. This polymer responded to applied NI radiation by releasing R848 into the tumour. This group also locally injected their formulation into the subcutaneous tumour core and achieved significant reduction in tumour growth, with 9 of 21 of mice displaying long term tumour immunity.

Despite the promising results of R848 as a TIME modulation agent, a key problem facing the use of this and other immune response modifiers is their delivery. In the Mullins and Chen study [37], R848-nanoparticles were locally injected into the tumour directly, likely due to the fact that systemic administration of immune response modifiers can induce "cytokine storms" where overproduction of inflammatory mediators can result in autoimmunity or dysfunction [39]. Moreover, R848 itself possess additional challenges in delivery as it is poorly soluble. An advanced delivery system for R848 to increase its solubility and target to the TIME is required to exert significant anti-tumour immune response.

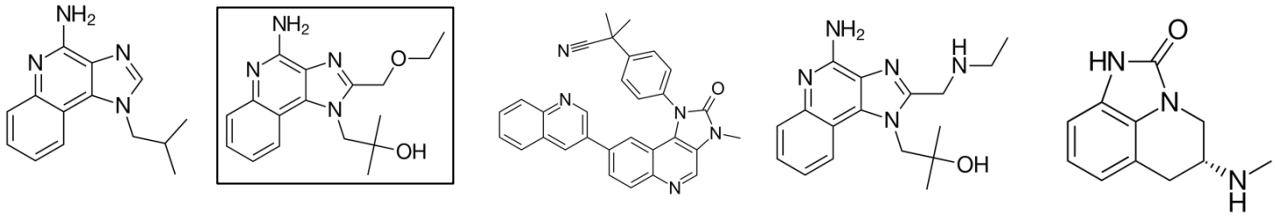

Figure 1. The imidazoquinolinone family. Imiquimod, Resiquimod (R848), Dactolisib, Gardiquimod and Sumanirole.

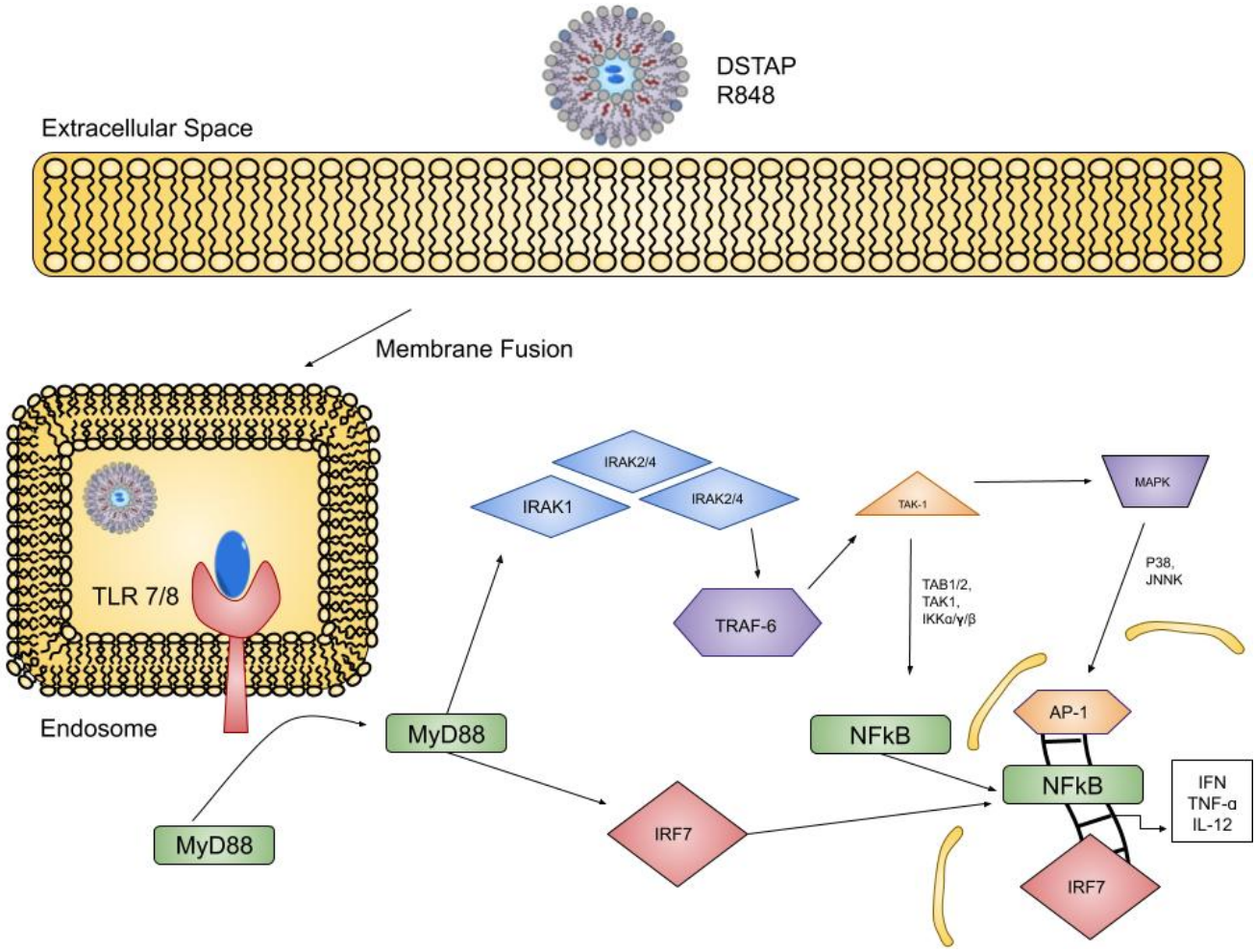

Figure 2. Molecular mechanisms of R848 in immune stimulation.

Table 1. Cytokines and Chemokines Induced by Imidazoquinolines

Interferons: ***IFN-α**, IFN-β
Interleukins IL-1, ***IL-6**, IL-8, IL-10, IL-12
Tumour necrosis factor-a ***TNF-α**
Interleukin 1 receptor antagonist IL-1RA
Granulocyte colony stimulating factor G-CSF
Granulocyte-macrophage colony stimulating factor GM-CSF
Macrophage inflammatory protein MIP-1a and MIP-1b
Macrophage chemotactic protein MCP

***Cytokines measured in this project**

Adapted from: M.A. Stanley, Imiquimod and the imidazoquinolones: Mechanism of action and therapeutic potential, Clin. Exp. Dermatol. 27 (2002) 571–577. https://doi.org/10.1046/j.1365-2230.2002.01151.x.

1.3 Liposomes

Liposomes are lipid-based spherical nanoparticles containing a bilayer structure which encloses an aqueous core**.** Hydrophobic drugs can be retained in the lipid bilayer and hydrophilic drugs can be encapsulated in the core. Drug loading of liposomes can be accomplished by passive loading, wherein the liposomes are formed and loaded concurrently. In contrast, liposomes can be actively loaded (otherwise known as remotely loaded). This process relies on production of empty liposomes and subsequent loading of a pharmaceutical agent via a transmembrane gradient. Active loading can achieve a higher drug-to-lipid ratio relative to passive loading, and generates a more stable formulation which does not undergo the "burst" drug leakage phenomena that occurs with passive loading [40]. With proper lipid composition and precise control of the physicochemical properties of liposomes, pharmacokinetics of an encapsulated drug and delivery to the target tissue/cell can be improved[41]. This project utilized two component lipids, shown below (**Figure 3 and Figure 4)** to form the bulk of the liposomal bilayer. Cholesterol was also included to improve the liposome stability. Cholesterol is believed stabilize liposomes by increasing the packing efficiency of phospholipids in the liposomal bilayer [42]. A schematic of the liposome generated in this projected is shown below in **Figure 5**.

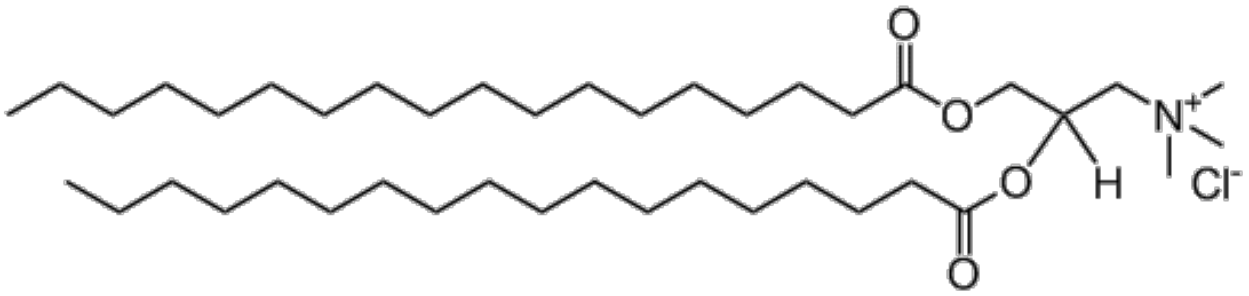

Figure 3. Chemical structure of cationic lipid 1,2-stearoyl-3-trimethylammonium-propane (chloride salt) (DSTAP) used in our liposomal formulation.

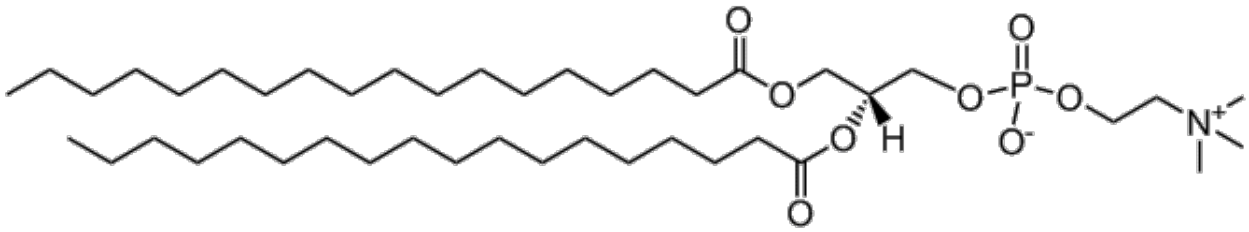

Figure 4. Chemical structure of helper lipid 1,2-distearoyl-sn-glycero-3-phosphocholine (DSPC) used in our liposomal formulation.

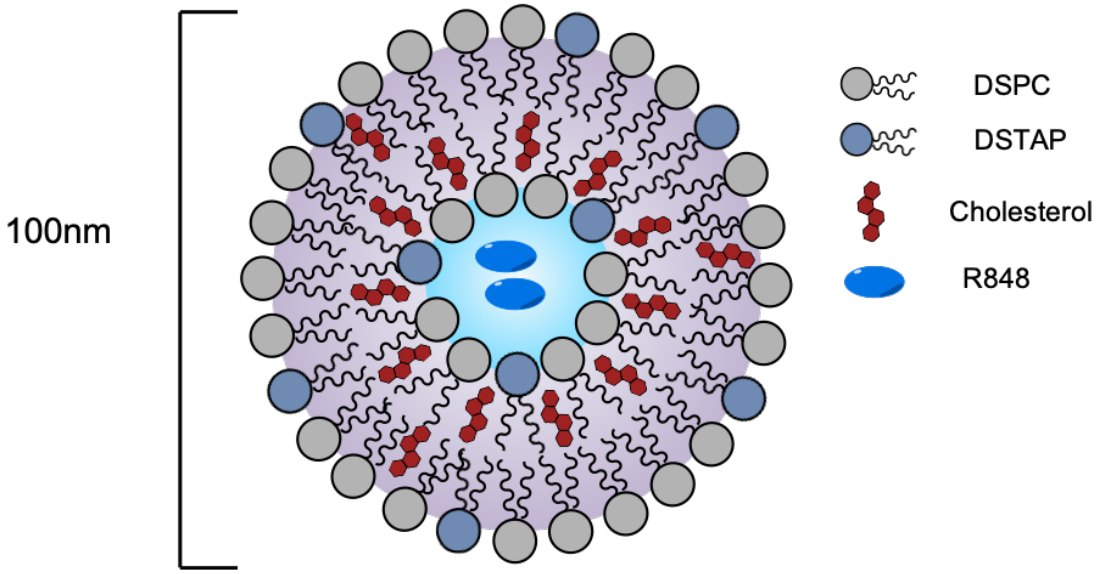

Figure 5. Schematic of DSTAP-liposome used in this study encapsulating R848.

1.4 Combination Therapy: Immunomodulatory and Cytotoxic Agents

The standard therapy for peritoneal metastases often includes chemotherapy, such as FOLFOX. FOLFOX contains folic acid, fluorouracil and oxaliplatin (OXA). In particular, OXA is known to induce immunogenic cell death, which triggers tumor antigen release to promote immune response. Antineoplastic agents can be synergistic with immune modulating agents due to the process of immunogenic cell death (ICD). In the context of cancer immunotherapy, the process of ICD describes the mechanism by which dying tumour cells can elicit an antitumor immune response[20].There are currently four types of ICD, that share common features described below[43] . It is believed this process evolved as a mechanism to mount an immune response against virally infected or mutated cells. ICD is characterized in part, by endoplasmic reticulum (ER) stress, exposure of calreticulin on the dying cell surface and the release of variety of antigenic molecules. The molecules released from the cell has been shown to correlate with the nature of the insult. In regard to chemotherapy induced ICD, common antigens include chromatin proteins (high mobility group box 1), intracellular nucleosides (adenosine triphosphate) and ER chaperones (calreticulin)[44] . These molecules bind with three innate immune receptors respectively; TLR 4, the purinergic receptor (P2Rx7) and CD91 expressed on the extracellular surface of immature dendritic cells. This initiates the maturation of DC and presentation of antigens to CTLs which then exert effector functions causing tumour cell lysis wherein the process begins anew. In 2013, Kromer et al. conducted a meta-analysis on 24 commonly used cytotoxic agents in oncology and found that only three anthracyclines and OXA were successful ICD inducers despite all being similar in ability to induce apoptosis in a mouse model [20]. The authors' criteria for a cytotoxic agent to be defined as an ICD inducer include only drugs that could produce sufficient antigen release from tumours that, when these dying cells were injected into a tumour bearing mouse, could decrease the tumour load and cause immunity from future tumour inoculation. As such, OXA is a powerful chemotherapeutic due to its ability to release antigens from tumour cells in addition to being used commonly in PC treatment. In order to take advantage of OXA's ICD effect, the addition of immune boosting agents could theoretically act synergistically by stimulating the production of inflammatory cytokines after antigen uptake and presentation has occurred.

1.5 Activating the Innate Immune Response

The innate immune system is composed of physical barriers, biochemical barriers, the complement system and the innate immune cells. These cells are subdivided into groups based on morphology and function. The innate immune cells include phagocytes (monocytes, macrophages, dendritic cells), mast cells, eosinophils, and natural killer cells. However, emerging research is beginning to "blur the line" between what constitutes an innate immune cell versus an adaptive one. For example, the gamma-delta T cell is often grouped with innate cells, but does possess a variable T cell receptor [22], similarly, NK cells are traditionally classified as innate despite sharing a common progenitor with T and B cells [45]. Further, recent evidence has discovered a subset of NK cells capable of antigen recognition and memory, acting similarly to CD8+ T cells [46]. As such, the innate immune system, NK cells in particular, are to receiving attention in the context of cancer immunotherapy due their ability to initiate the adaptive response and perform tumour lysis [47,48]. In mice, NK cells originate in the bone marrow and traffic to secondary lymph organs where they can further mature, expressing a range of cell surface markers classifying them as immature NK (iNK NK1.1+), mature NK (mNK Nkp46/CD335+) and NKT (abTCR) cells [45]. These cells share overlapping functions with both cytotoxic T cells and antigen presenting cells in that they can both lyse transformed cells and secrete cytokines to prime the adaptive immune system. Most NK cells distinguish transformed cells from healthy cells via the presence of "self-molecules" such as MHC-1, which acts as a strong inhibitory signal when detected on healthy cells. This process is also known as the "missing self-recognition theory" whereby the extinction of expression of polymorphic MHC molecules on target cells frees the contact dependent inhibition on NK cell and allows them to release cytotoxic granules aimed at this target. However, recently some NK subsets have been found to express no inhibitory receptor to MHC and are hyperresponsive to stimulation [49]. The MHC-1 complex is often down regulated in tumour cells [50]. To contribute to the immune response, NK cells require the absence of inhibitory MHC-1 and the stimulation of cytokines TNF-α, IL-12. If these conditions are met, NK cells act through the Th_1 response and secrete large amounts of IFN-γ, TNF-α and granulocyte/monocyte-CSF. However, their true potential in regard to tumour immunosurveillance lies in

the innate ability to secrete cytotoxic granules such as perforins. As early as 1980, NK cells were recognized for their ability to protect against tumour peritoneal cancer inoculation and their induction could prolong survival in cancer laden mice [51]. More recently, NK cells have been used in allogeneic cancer immunotherapy in the clinic where the highly cytotoxic human NK cell line, NK92, is cultured , expanded and primed before it is re-injected into the patient [52]. There have been a number of clinical trials on NK cell therapy, see Guillerary et al. 2016. These trials have not been overwhelmingly positive. A major issue facing the NK cell therapy landscape is the overstimulation of NK cells *in vitro* prior to re-injection [53]. This overstimulation can cause graft-versus-host disease, where NK cells attack healthy tissues. Therefore, NK cell therapies could be advanced through the introduction of a technology which could boost NK, B and T cell, activity *in vivo* and remove the barriers faced with extraction, propagation, stimulation, and re-injection used in traditional allogeneic therapies.

1.6 Research Hypothesis and Aims of Thesis

We hypothesized that cationic liposomes could be used to encapsulate R848, thus overcoming its poor solubility and increasing peritoneal retention following IP injection. This could lead to enhanced modulation of the peritoneal TIME, improved anti-tumour efficacy, and reduced systemic absorption of R848. This new formulation for R848 will enhance the immunotherapy of PC. We used DSTAP, a cationic lipid, to prepare a positively charged liposome for delivery of R848. The project contains two specific aims:

1. Compare pharmacokinetics (PK) and biodistribution (BD) of DSTAP-R848 and free R848 following IP delivery
    1.1. Preparation and characterization of DSTAP-R848
    1.2. PK and BD analysis of DSTAP-R848 and free R848
    1.3. Immune cell uptake of DSTAP-R848 in the peritoneal cavity
2. In vivo efficacy and mechanistic study of DSTAP-R848 relative to free R848 and vehicle control

2.1. *In vivo* gene expression and cytokine induction from DSTAP-R848 and free R848

2.2. Efficacy and tolerability study of DSTAP-R848 vs free R848 in a murine PC model

2.3. Immune cell modulation in the peritoneal cavity after DSTAP-R848 and free R848 treatment

Chapter 2: Materials and Methods

2.1 Materials

Cholesterol was purchased from Sigma Aldrich (St. Louis, MO)1,2-stearoyl-3-trimethylammonium-propane (chloride salt) (DSTAP) and 1,2-distearoyl-sn-glycero-3-phosphocholine (DSPC) and 1,2-distearoyl-sn-glycero-3-phospho-(1'-rac-glycerol) (sodium salt) (DSPG) were purchased from Avanti Polar Lipids, (Alabaster, AL). Resiquimod (R848) was obtained from Cayman chemicals (Ann Arbor, MI). Acetic acid, dimethyl sulfoxide, sodium acetate, sodium sulfate, ammonium thiocyanate, and ferric chloride were purchased from Sigma Aldrich, (St. Louis, MO). Dil (1,1'-Dioctadecyl-3,3,3',3'-Tetramethylindocarbocyanine Perchlorate) and DiR (1,1'-Dioctadecyl-3,3,3',3'-Tetramethylindotricarbocyanine Iodide) stain was purchased from Thermo Fischer Scientific (Toronto, ON, Canada). Luciferase plasmid (Plasmid # 18964) was obtained from Addgene (Watertown, MA). The transfection reagent, Turbofectin, was ordered from Origene (CAT#: TF81001) (Rockville, MD) and polybrene from Sigma-Aldrich (St. Louis, MO).

2.2 Liposome Preparation and Characterization for DSPC, DSPG and DSTAP Liposomes

Lipids cholesterol, DSPC, DSPG, were dissolved in chloroform and DSTAP was dissolved in chloroform:methanol (5:1). Lipid constituents were then mixed according to a molar ratio of (2X:1Y:0.8Z) where X= DSPC, Y=DSTAP/DSPG and Z=cholesterol. A thin lipid film was produced by rotary evaporation under vacuum at 60°C. The thin film containing 50 mg DSPC, 12 mg DSTAP and 18 mg cholesterol was hydrated with 2 mL of 300 mM ammonium sulfate (NH_4S0_2) (pH 5) and the lipid mixture was extruded while heated at 60°C progressively through 400, 100, and 50 nm polycarbonate membranes using the Avanti Mini-Extruder (Alabaster Alabama, USA) obtain liposomes with a monodispersed particle size. Liposomes were then transferred to a dialysis membrane (Spectrum Laboratories, Rancho Domingues, CA) and placed in acetate buffer (acetic acid 17.5 mL, sodium acetate

57.66 g NaCl 46 g in 1 litre of MilliQ) adjusted to pH=5.0 and dialyzed for 24 h while acetate buffer was replaced at 2 h and 4 h then left overnight. Liposomes were then characterized by size, polydispersity index (PDI) and zeta potential (ZP) using the Zetasizer Nano ZS, (Malvern Instruments Ltd. Malvern, UK). Lipid concentration was determined using the Stewart assay (described below) or ultra-high-performance liquid chromatography coupled to electron light scattering detection (UPLC-ELSD) as described below.

2.3 DiI-Liposome Preparation for *In Vitro* and *In Vivo* Uptake Studies

Cholesterol, DSPC and DiI were dissolved in chloroform and DSTAP was dissolved in chloroform: methanol (5:1). Lipid constituents (DSPC, DSTAP, Chol, DiI) were then mixed according to a molar ratio of 2:1:0.8:0.05. Liposomes were prepared by combining 920mL of 50mg/mL DSPC, 360 µL of 50mg/mL DSTAP and 240 µL of 50mg/mL cholesterol and 80µL of DiI, for a final volume 1.5mL. A thin film was formed using rotary evaporation at 60°C. The thin film was hydrated with 2 mL of 300 mM ammonium sulfate (NH_4S0_2) (pH 5) and the lipid mixture was extruded while heated at 60°C progressively through 400, 100, and 50 nm polycarbonate membranes using the Avanti Mini-Extruder (Alabaster Alabama, USA) obtain liposomes with a monodispersed particle size. The liposomes were then dialyzed as described previously in acetate buffer then glucose to mirror previous studies.

2.4 R848 Loading Into DSTAP-liposomes

R848 was dissolved in DMSO at 40 mg/mL and then diluted with acetate buffer (300 mM, pH 5) to 4 mg/mL before being added into the DSTAP-liposomes at a drug-to-lipid ratio of 1:5 w/w. The mixture was incubated at 60°C in a metal heating block for 30 min then cooled rapidly on ice for 3 min. The freshly loaded particles were then placed in a dialysis bag and dialyzed against 5% glucose solution (10x volume of the particles) for 24 h with two changes of the dialysate at 2 h and 4 h to remove DMSO and unencapsulated R848. Again, lipid and R848 concentrations in the final DSTAP-R848 product was

measured using the Stewart assay and UPLC-ELSD (below). Particle size, PDI and ZP of DSTAP-R848 were measured by DLS as described previously.

2.5 Stewart Assay

The Stewart away is a colometric assay that quantifies phospholipids based on their ability to form color complexes with ammonium ferrothiocyanate. The ferrothiocyante solution is made by dissolving 27.03 g of ferric chloride hexahydrate (Sigma Aldrich, St Louis, MO) and 30.4 g of ammonium thiocyanate (Sigma Aldrich, St Louis, MO) in 1 L of MilliQ. The solution is stable at room temperature for several months. A range of 5 solutions was generated to form the standard curve. The sample solution was prepared by diluting 5 uL of liposome solution with 1995 uL chloroform (40X dilution). The sample solution was then added to a glass tube containing 2 mL of the ferrothiocyante solution. The tube was then capped and vortexed for 30 s, centrifuged at 300 g for 10 min, and the optical density at 485 nm of the supernatant was determined by a spectrophotometer. The result was then compared to the calibration curve to estimate the lipid concentration of liposomes.

2.6 UPLC Characterization of Liposomes

Liposomes were dissolved in methanol (1:10) and sonicated for 10 min, and 10 µL of the sample was analyzed using a Waters ACQUITY UPLC H-Class system (Milford, MA). The sample was separated on a Waters Acquity BEH-C18 column (particle size: 1.7 µm inner diameter: 2.1 mm length: 100 mm column) at a flow rate of 0.4 mL/min. Samples were separated on a Waters Acquity BEH-C18 column (particle size: 1.7 µm inner diameter: 2.1 mm length: 100 mm column) at a flow rate of 0.4 mL/min. The mobile phase was comprised of solvent A (0.1% formic acid in water, v/v) and solvent B (aqueous 90% acetonitrile containing 0.1% formic acid, v/v). The following gradient was applied: 3.0 min: A/B (95/5), 11.0 min: A/B (47/53), 12 min: A/B (5/95), 13.0 min: A/B (5/95), 13.5 min: A/B (95/5), 15.0 min: A/B (95/5). The mass spectrometer was operated in the positive ionization mode. Ionization was carried out at

450 °C (source temperature) using a cone voltage of 25 kV. The R848 concentration was determined by integrating the single ion recognition (SIR) peak for the singly charged molecular ion as m/z 315 and calibrated 30 μL, 1 mg/L Mefloquine in 90% aqueous acetonitrile, v/v, as internal standardwith the SIR peak at m/z 379. Data was analyzed using the Empower 3.0 software (Waters).

2.7 Cell Culture

Raw 264.7 cells (macrophage) and CT-26 murine colorectal cells were obtained from American Type Cell Collection (Gaithersburg, ML) and propagated in Dulbecco's Modified Eagle Medium (DMEM) supplemented with 5% fetal bovine serum (FBS) and 1% penicillin/streptomycin. Generation of the luciferase expressing CT-26 (CT-26-Luc) cell line was achieved by using a lentiviral vector containing a luciferase gene with neomycin resistance (described below). Luciferase expressing cells were selected under a culture medium containing 1000 μM of neomycin.

2.8 Cellular Uptake of DiI-Liposomes

Raw 264.7 cells (50,000/well) were added to a 24-well plate containing a glass coverslip in each well. Cells were left to adhere to the coverslip for 12h. The medium was removed, and cells were washed gently 3 times with cold PBS. DiI-labled liposomes were added at a concentration of 0.5 μg/mL to each well and allowed to incubate for 1 h, 4 h, and 24 h. Cells were then washed gently with cold PBS for three times. Lysotracker Green was added at a concentration of 50 nM and incubated for 1 h. Cells were then fixed with 10% formalin solution for 15 min. Fixed cells were washed again with PBS and the glass coverslip was mounted onto a glass slide with mounting medium containing 4′,6-diamidino-2-phenylindole (DAPI). Slides were then imaged on FluoView A confocal microscope (Olympus). Intensity of DiI and DAPI signal was measured using ImageScope software with the positive pixel count algorithm.

2.9 Mice

Female BALB/C and CD1 (6-8 weeks old) were purchased from the Jackson Laboratory and housed according to the institutional guidelines. Food and water was provided ad libitum. All animal experiments were conducted with an approved protocol A18-0177 at the University of British Columbia.

2.10 Pharmacokinetic and Biodistribution Studies

Free R848 and DSTAP-R848 (1 mg R848/kg) were injected intraperitoneally (IP) into female CD1 mice (25-30 g, 6-7 weeks old, Charles River Laboratories, Senneville, QC, Canada). At different timepoints (15 min, 1 h, 4 h, and 24 h), blood was collected via cardiac puncture through the skin, then the mice were euthanized and peritoneum fluid (PF, original volume ~100 µl) was expanded and effectively collected after IP instillation with 2 mL phosphate-buffered saline PBS. Plasma was obtained by centrifuging (5000 rpm, 10 min) blood immediately after collection in K_2-ethylenediaminetetraacetate collection tubes (Microvette, Sarstedt AG & Co., Nümbrecht, Germany), and IP cells (cells in PF) were isolated from PF through centrifugation (1500 rpm, 5 min).

R848 was extracted from plasma, PF, and IP cells, followed by analysis using ultra performance liquid chromatography (UPLC). Briefly, IP cells were pretreated with 1% aqueous Triton-X solution (50 µL, v/v) for 15 min on ice and spun (12,500 rpm, 10 min) to harvest the supernatant. Analytes were extracted by mixing plasma, PF, or IP cell lysate (45 µL) with Mefloquine solution (30 µL, 1 mg/L Mefloquine in 90% aqueous acetonitrile, v/v, as internal standard) and cold 90% aqueous acetonitrile (270 µL, v/v) respectively. The mixture was vortexed for 30 seconds, placed on ice for 30 min, and centrifuged (12,500 rpm, 5 min). The supernatant (300 µL) was collected, lyophilized, and rehydrated in 4.5% aqueous acetonitrile with 0.1% formic acid (60 µL, v/v). Samples were injected (10 µL) into a Waters ACQUITY UPLC H-Class system (Milford, MA) coupled on-line to a Waters QDa mass spectrometry detector. Samples were separated on a Waters Acquity BEH-C18 column (particle size: 1.7 µm inner diameter: 2.1 mm length: 100 mm column) at a flow rate of 0.4 mL/min. The mobile phase was comprised of solvent A (0.1% formic acid in water,

v/v) and solvent B (aqueous 90% acetonitrile containing 0.1% formic acid, v/v). The following gradient was applied: 3.0 min: A/B (95/5), 11.0 min: A/B (47/53), 12 min: A/B (5/95), 13.0 min: A/B (5/95), 13.5 min: A/B (95/5), 15.0 min: A/B (95/5). The mass spectrometer was operated in positive ionization mode. Ionization was carried out at 600°C (source temperature) using a cone voltage of 15 V and a capillary voltage of 0.8 kV. The R848 concentration was determined by integrating the single ion recognition (SIR) peak for the singly charged molecular ion as m/z 315.0 and calibrated by Mefloquine with the SIR peak at m/z 379.1. Data was analyzed using the Empower 3.0 software (Waters).

2.11 Immune Stimulation Cytokine Studies

Cytokine production and secretion in the plasma, PF, and IP cells induced by free R848 or DSTAP-R848 was measured by ELISA or real-time polymerase chain reaction (RT-PCR). After collection from the IP fluid, cells were lysed and mRNA was extracted and purified using the PureLink RNA mini kit from Ambion Life Technologies (Thermo Fisher, Toronto ON, Canada) following manufactures guidelines for cell suspensions. mRNA retrieved from the IP cells was then used in the high-capacity cDNA reverse transcription kit from Applied Biosystems (Thermo Fisher, Toronto ON, Canada) per manufactures guidelines. mRNA levels of key mouse cytokines including IFN-α, IL-6, and TNF-α in the IP cells were determined by RT-PCR using the comparative Ct method (GAPDH as internal control). The primer sequences of these markers were listed in Table 1. IFN-α level in plasma and PF was measured using the ELISA kit (eBioscience) following the manufacturer's instruction.

Table 2. Primer sequences for RT-PCR.

Gene	Primer	Sequence (5'-3')
GAPDH	F	AGGTCGGTGTGAACGGATTTG
	R	TGTAGACCATGTAGTTGAGGTCA
IFN-α	F	GAATGCAACCCTCCTAGAC
	R	GTCAGAGGAGGTTCCTG
IL-6	F	TAGTCCTTCCTACCCCAATTTCC
	R	TTGGTCCTTAGCCACTCCTTC
TNF-α	F	CCCTCACACTCAGATCATCTTCT
	R	GCTACGACGTGGGCTACAG

2.12 Luciferase Gene Transduction in CT-26 cells

To prepare the in-house lentiviral vector for luciferase gene transduction, HEK293 T cells were transfected with Turbofectin complexed with a neomycin-resistant luciferase pDNA containing three major viral structural genes: gag, pol, and env. After 24 h and 48 h, the viral particle rich media was collected, centrifuged and stored in -80ºC. On the day of infection, CT-26 cells in a T-75 flask were incubated with 750 uL of the viral particles and polybrene. On the next day, media was replenished, and cells were selected under neomycin resistance at 700 μg/mL.

2.13 In Vivo Efficacy and Imaging

Female 6-8-week-old BALB/C mice (approximately 20g) were IP inoculated with 2×10^5 CT-26-Luc cells on day -4. On day 0, mice were injected with 15mg/kg luciferin dissolved in PBS and then imaged using the Xengoen IVIS system after 15 minutes to confirm the presence of tumours in peritoneal cavity. Mice with roughly equal levels of bioluminescent tumour expression were then assigned randomly to three groups. On day 1 all mice received 6mg/kg OXA. On day 2, mice received one of either 8mg/kg free R848, 8mg/kg DSTAP-R848 or equivalent volume of PBS solution. Mice were then imaged every day for

the next three days to monitor tumour progression. Subsequently, mice were imaged every 2 days to monitor tumour growth until the study endpoint day 14. Mice were then imaged, sacrificed, and the tumours were collected.

2.14 Flow Cytometry Analysis of Cellular uptake of DSTAP-liposomes by IP cells

Mice were IP inoculated with 2×10^5 CT-26-Luc cells on day -4. On day 0, mice were imaged by the IVIS Xenogen 15 min after IP injection of 15 mg/kg luciferin to confirm tumour presence. Mice then received 8 mg/kg OXA via IP injection. The following morning, each mouse received an IP injection of 200 uL of DiI-labelled DSTAP-liposomes (10 mg/kg lipid). After 1 h, mice were sacrificed, and the IP fluid was retrieved by installation of 5 mL ice-cold PBS. The IP fluid was then centrifuged and the supernatant aspirated. The IP cells were resuspended in a staining buffer (PBS containing 1% bovine serum albumin (or 4% fetal calf serum) and 0.05% Sodium Azide), counted and dispensed into an Eppendorf tube and stained with various antibodies (anti-CD45, anti-CD11b, anti-CD11c, anti-F4/80, anti-CD335, anti-CD3, anti-CD8, and anti-EPCAM) for 30 min on ice in the dark. The cells were centrifuged again, resuspended in the fluorescence activated cell sorting buffer (Thermo Fisher, St Louis MO) containing 1 mg/ml propidium iodide, and analyzed by the Beckman Coulter Cytoflex LX.

2.15 Statistical Analysis

All data are expressed as mean ± SD. Statistical analysis was conducted with the two-tailed unpaired *t* test for two-group comparison or one-way ANOVA, followed by the Tukey's multiple comparison test by using GraphPad Prism (for three or more groups). A difference with P value < 0.05 was considered to be statistically significant.

Chapter 3: Results and Discussion

3.1 Aim 1: Comparing pharmacokinetics (PK) and biodistribution (BD) of DSTAP-R848 and free R848 following IP delivery.

3.1.1 Peritoneal Retention of Liposomes

Liposomes can be formulated to have an array of physicochemical properties. Modulation of lipid constituents influences the size, surface charge, polydispersity index (PDI) and drug release kinetics [54]. This can, in turn, impact the pharmacokinetic and biodistribution profiles of liposomes and their encapsulated drugs [55]. Three liposomal formulations containing a fluorescent dye (DiR) with different surface charge characteristics (neutral: DSPC; cationic: DSTAP; negative: DSPG) were prepared to compare their peritoneal retention. Their formulations and physicochemical properties including size, polydispersity index and zeta potential are summarized in **Table 3**. As shown in Table 3, these three formulations showed a comparable mean diameter, in the range of 80 nm and were all monodispersed based on the low PDI value <0.1. However, the formulations differed in their respective zeta potential (ZP). As predicted, the formulation containing the negatively charged lipid DSPG, showed an anionic ZP at -42.9 mV. The formulation containing only neutral lipid DSPC demonstrated a neutral ZP at 7.9 mV. Lastly, the formulation containing the cationic lipid DSTAP demonstrated a highly positive ZP at 51.3 mV. To investigate the impact of ZP variations on the peritoneal retention, these three formulations were IP injected into 9 mice (n=3 per group), and their peritoneal retention over time was quantified by Xenogen IVIS imaging. As shown in **Figure 6,** all formulations were initially confined to the peritoneal cavity. However, after 1 h, the neutral (7.9 mV) DSPC formulation and negative (-42.9 mV) DSPG formulations rapidly began to enter the systemic circulation as depicted by the spreading DiR signal over 1-24 h. In contrast, the cationic (51.3 mV) DSTAP-liposomes exhibited enhanced peritoneal retention up to the study endpoint of 24 h. This is likely due to the fact that cationic DSTAP-liposomes could rapidly interact with negatively charged cell membrane of the IP cells and the peritoneal lining [54]. Owing to its

ability to focus the delivery to the peritoneal cavity, we then selected the DSTAP-liposomal formulation for delivery of R848 for treating peritoneal tumours.

Table 3. Physiochemical characteristics of three different liposomal formulations

Liposome	Formulation Chemical Ratios	Size (nm)	PDI	Zeta Potential (mV)
Cationic (DSTAP) Liposomes	DSPC/ DSTAP/ Chol/ /DiI Mol Ratio (0.52:0.21:0.26:0.01)	79.57 ± 6.12 nm	0.047 ± 0.017	51.3 ±2.940
Neutral (DSPC) Liposomes	DSPC/Chol/DiI Mol Ratio (0.73:0.26:0.01)	80.79 ± 19.31 nm	0.063 ± 0.030	7.19 ± 1.98
Anionic (DSPG) Liposomes	DSPC/ DSPG/ Chol/DiI Mol Ratio (0.52:0.21:0.26:0.01)	84.57 ± 5.70 nm	0.016 ± 0.0091	-42.9 ± 0.350

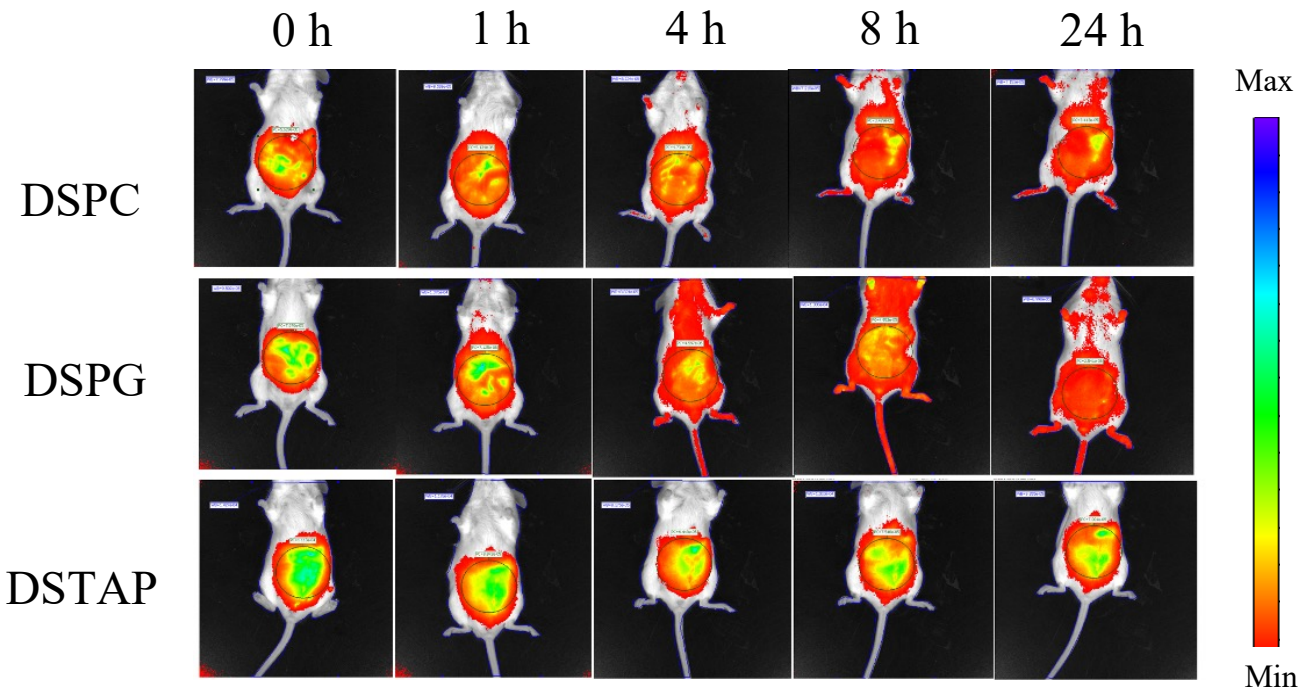

Figure 6. Representative images of the distribution of DiR labelled liposomes (DSPC, DSPG, and DSTAP) in the mouse peritoneal cavity over 24 h.

3.1.2 In Vitro Cellular Uptake of DSTAP-Liposomes

To demonstrate that DSTAP-liposomes could deliver R848 to the endosomes and facilitate activation of the TLR7/8 we conducted *in vitro* uptake studies. DSTAP-liposomes were labeled with a fluorescent lipid DiI and incubated with Raw 264.7 cells, followed by confocal microscopic imaging. As shown in **Figure 7**, DiI-DSTAP-liposomes were highly co-localized with the endosomes/lysosomes, where TLRs 7/8 reside. The data indicate that the DSTAP-liposomes targeted R848 to the desirable sub-cellular compartment.

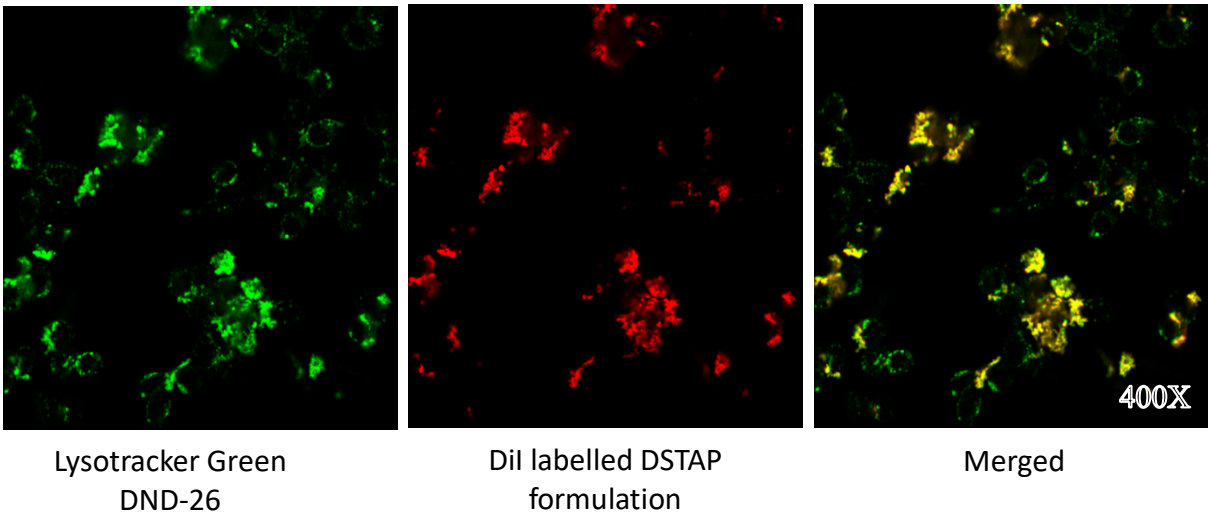

Figure 7. Confocal microscopic images of Raw 264.7 cells after incubation with DiI-DSTAP-liposomes. Red: DiI-DSTAP-liposomes; Green: LysoTracker Green; Yellow: overlay.

3.1.3 R848 Loading into DSTAP-Liposomes

R848 is a poorly water-soluble compound [56]. To effectively load R848 into DSTAP-liposomes, our lab has developed the solvent-assisted active loading technology (SALT) [40]. In brief, SALT involves using a small amount of water-miscible solvent during the drug loading process to increase the drug solubility and membrane permeability, facilitating the loading of a poorly soluble drug into the aqueous core of liposomes. DSTAP-R848 liposomes were characterized by dynamic light scattering, Stewart assay and UPLC to measure its size, PDI, zeta potential, lipid concentration, drug concentration and drug encapsulation efficiency. As shown Table 4, the R848 concentration was approximately 1.76 mg/mL and the total lipid concentration as approximately 9.59 mg/mL. R848 was readily encapsulated inside DSTAP-liposomes as we achieved a loading efficiency of 80.24%. The mean diameter of the DSTAP-R848 liposomes was 104 nm, a slight increase from the empty DSTAP-liposomes. This finding is in accordance with our previous studies and the literature [57], and the size increase could be due to drug

molecule aggregation inside the liposomes, expanding the structure. The DSTAP-R848 liposomes displayed a monodispersed population as the PDI remained below 0.1, with a positive ZP of 43.02mV.

Table 4. Characterization of DSTAP-R848 from 3 batches

Drug Conc (mg/mL)	Total Lipid Conc (mg/mL)	Loading Efficiency (%)	Size (nm)	(PDI)	Zeta Potential (mV)
1.76 ±0.64	9.59 ± 2.06	80.24 ± 3.2%	104.6 ±7.2	0.084 ± 0.006	43.02 ± 5.32

3.1.4 PK and BD Analysis of DSTAP-R848 and Free R848

We next compared the pharmacokinetic and biodistribution profiles of free R848 and DSTAP-R848 in a mouse model. After IP administration of either free drug or DSTAP-R848, we collected blood via the saphenous vein at various time points. We also collected the IP fluid to investigate the peritoneal retention. Lastly, we retrieved IP cells from the peritoneal fluid to study the immune cellular uptake of the two formulations of R848. As shown below in **Figure 8A and Table 5**, mice treated with DSTAP-R848 displayed ~14-fold increased dose exposure in the PF (calculated as the area under the curve, $AUC_{0.25\text{-}4h}$) relative to free drug that was removed from the peritoneum within 1 h. Accordingly, within 15 min post injection, free R848 was absorbed into the blood, achieving a C_{max} of 0.3 μg/mL, while the plasma C_{max} in the DSTAP-R848 group occurred at 1 h with a 5-fold reduced concentration **(Figure 8B**). However, the AUC_{plasma} was comparable between the two groups (Table 5). This is likely due to a delayed absorption effect that is shown by a rapid spike leading to a high C_{max} value in the free drug group relative to a slower increase over the first hour in the DSTAP formulation in Figure 9B. The drug exposure ratios (PF/plasma) for DSTAP-R848 and free R848 were ~680 and ~45, respectively (Table 5). Lastly, R848 in the IP cell pellets collected from the PF was under the detection limit in the free drug group, while a

significant amount of R848 (0.1-0.5 µg) was determined in the DSTAP-R848 group during the first hour post IP injection (**Figure 8C**). Accordingly, the DSTAP formulation caused a significant increase in the $AUC_{0.25\text{-}4H}$ concentration of R848 in the IP cells at 0.4604 µg/ml x h relative to free drug which remained undetectable.

Overall, the data indicate that free R848 was rapidly absorbed from the peritoneum into the blood circulation, with poor IP retention and uptake by the IP cells. In contrast, DSTAP-R848 effectively retained in the peritoneum and displayed increased delivery to the IP cells compared to free R848, with delayed systemic absorption, which could be beneficial for reducing global TLR7/8 activation.

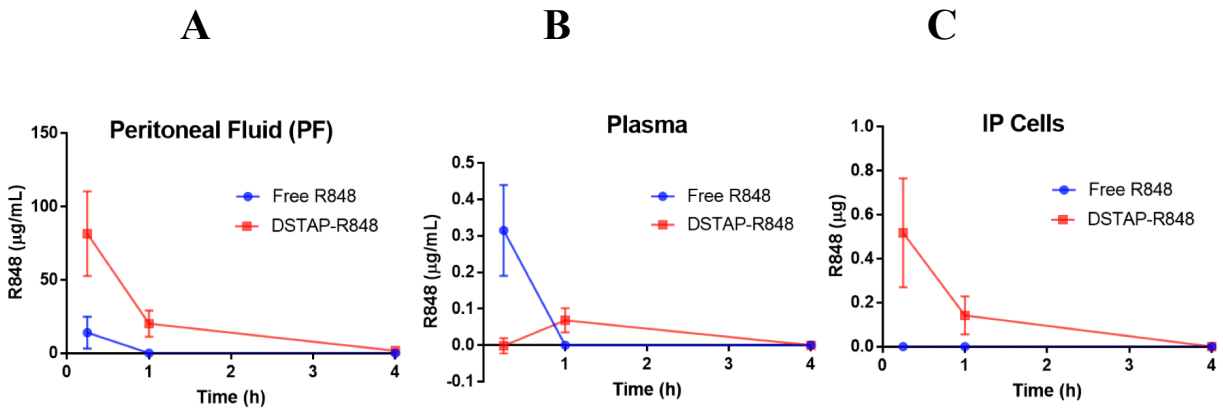

Figure 8. Pharmacokinetics and biodistribution of free R848 and DSTAP-R848 in mice after IP administration. A) R848 concentrations in the peritoneal fluid after IP injection of DSTAP-R848 or free R848 (Data = mean ± SD, n=5). B) Plasma R848 concentrations after IP injection of DSTAP-R848 or free R848 (Data = mean ± SD, n=5). C) R848 concentrations in the IP cells after IP injection of DSTAP-R848 or free R848 (Data = mean ± SD, n=5).

Table 5. Area Under the Curve for Figure 8.

Parameter	Free R848	DSTAP-R848	Significance
$AUC_{0.25\text{-}4H}$ Peritoneal Fluid	5.292 ± 4.099 (h • μg/mL)	71.06 +/- 17.7 (h • μg/mL)	P<0.005
$AUC_{0.25\text{-}4H}$ Plasma	0.1181 +/- 0.04669 (h • μg/mL)	0.1288 +/- 0.05111 (h • μg/mL)	NS
$AUC_{0.25\text{-}4H}$ IP cells	0 (below detection limit)	0.4604 +/- 0.1638 (h • μg/mL)	P<0.005

TLR agonists such as R848 are typically administered topically or locally such as intratumoural injection to avoid systemic toxicity [58]. As stated in a recent review by Dowling 2018 [59], R848 requires optimization of its PK profile before being able to be administered systemically (e.g. IV or IP). In this study we aimed to develop a liposomal formulation to confine R848 in the peritoneal cavity for treating PC while minimizing the systemic distribution. We hypothesize that this would allow localized activation of the immune system in the TIME to improve treatment of PC. Overall, this was achieved using the DSTAP-liposome formulation.

3.1.5 *In Vivo* Immune Cell Uptake of DSTAP-Liposomes

As we demonstrated that the DSTAP formulation was able to boost the delivery of R848 to the IP cells relative to free drug, we sought to further characterize which cells in the peritoneum were responsible for this uptake. DSTAP-liposomes were labeled with 0.5 mol% of DiI and IP injected into tumour bearing

mice (n=3) to mirror the efficacy and tolerability studies. The IP fluid was retrieved 60 min post injection, and the IP cells were collected, stained using fluorescent antibodies, and analyzed by flow cytometry. After selecting singlets using forward scatter by side scatter, we selected only live, DiI+ cells and then examined the immune cell populations (**Figure 9A**). This was achieved by including only those that were both propidium iodide negative and DiI+. The peritoneum is mainly populated by monocytes, macrophages, dendritic cells and a population of B cells [60,61]. We found that the monocyte population ($CD45^+$, $CD11b^+$, $CD3^-$, $CD19^-$, $CD11c^-$, $F4/80^-$) accounted for ~50% of the DiI+ IP cells. In addition, approximately 10% and 8% of the DiI+ IP cells were myelogenous dendritic cells ($CD45^+$, $CD11b^+$, $CD11c^+$) and NK cells ($CD45^+$, $CD11b^+$, $CD11c^-$, $NKp46/CD335^+$), respectively (**Figure 9B**). We further investigated the DiI+ populations using the cell surface marker F4/80, which is found on large-type peritoneal macrophages (LPM) ($CD45^+$, $CD11b^+$, $F4/80^+$), a distinct subset of a multi-focal family of macrophages and monocytes [62], and found that the uptake by the LPM was negligible. Interestingly, we did not observe any significant amount of DiI+ B cells ($CD45^+$, $CD11b^+$, $CD3^-$, $CD19^+$), this is likely due to their small population size and limited phagocytic activity in higher order mammals [63–65]. However, like B cells, NK cells also have limited phagocytic activity, and as such, their representation among DiI positive cells may be due to a high non-specific uptake if their population size was sufficiently large. Overall, it appears that DSTAP-liposomes were selective for monocytes, small-type peritoneal macrophages (CD45+, Cd11b+, F4/80-), dendritic cells ($CD45^+$, $CD11b^+$, $CD11c^+$) and NK cells ($CD45^+$, $CD11b^+$, $CD11c^-$, $NKp46/CD335^+$).

A)

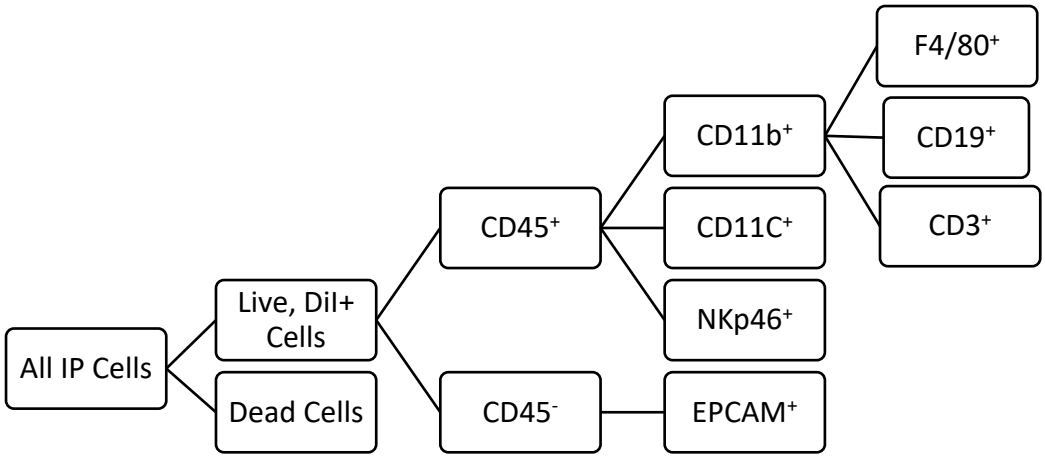
All IP Cells
Live, DiI+ Cells
Dead Cells
CD45+
CD45-
CD11b+
CD11C+
NKp46+
EPCAM+
F4/80+
CD19+
CD3+

B)

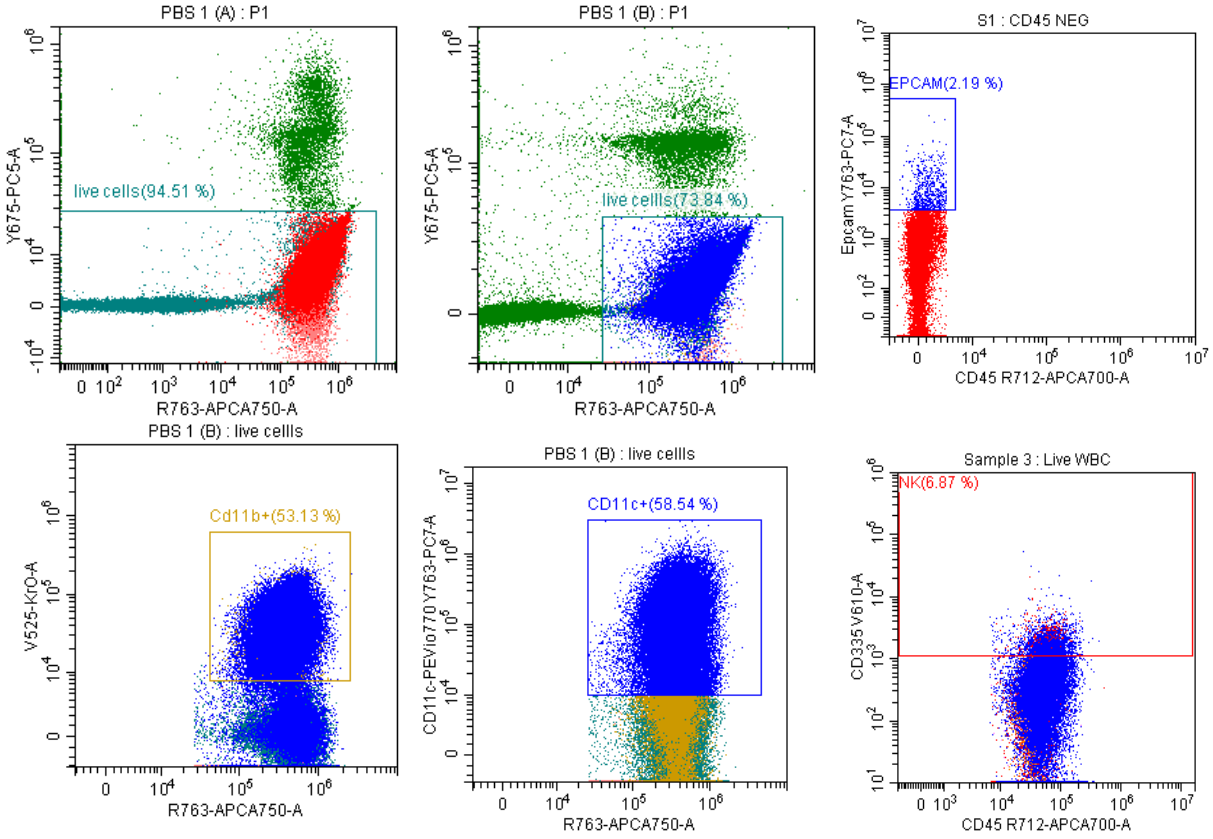
PBS 1 (A) : P1
live cells(94.51 %)
Y675-PC5-A
R763-APCA750-A
PBS 1 (B) : P1
live cellls(73.84 %)
Y675-PC5-A
R763-APCA750-A
S1 : CD45 NEG
EPCAM(2.19 %)
Epcam Y763-PC7-A
CD45 R712-APCA700-A
PBS 1 (B) : live cellls
Cd11b+(53.13 %)
V525-KrO-A
R763-APCA750-A
PBS 1 (B) : live cellls
CD11c+(58.54 %)
CD11c-PEVio770 Y763-PC7-A
R763-APCA750-A
Sample 3 : Live WBC
NK(6.87 %)
CD335 V610-A
CD45 R712-APCA700-A

C)

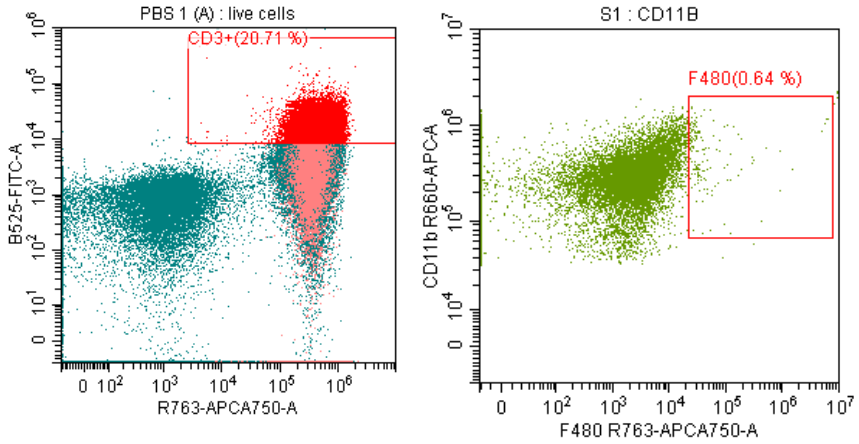

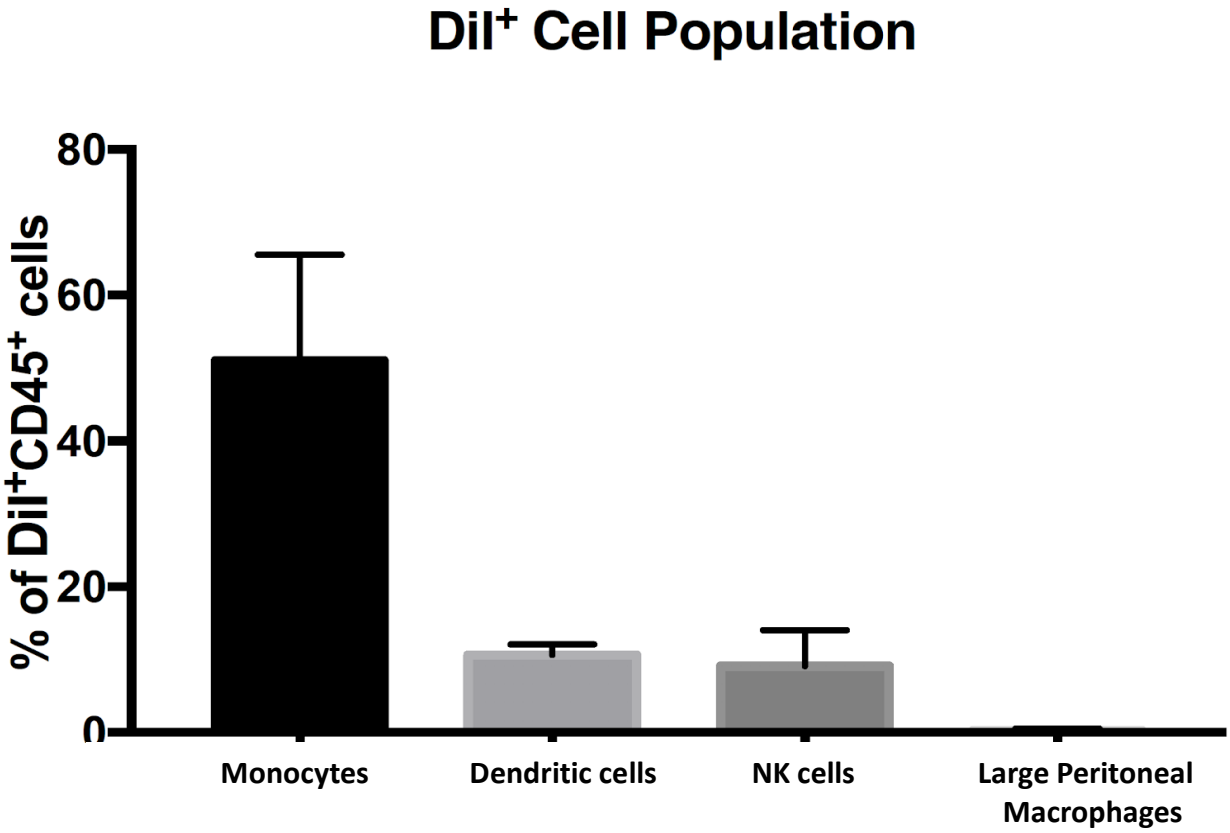

Figure 9. Flow cytometry analysis of DiI-DSTAP-liposome uptake by the IP immune cells.

A) Schematic of the gating protocol used in FACS to measure DiI+ cells retrieved from the peritoneal cavity. **B**) Representative flow cytometry plots demonstrating gating strategy **C)** Graphical representation

of DiI+ immune cell populations in the peritoneal cavity. Expressed as percentage (Data = mean ± SD, n=3).

Despite their role as scavenger cells and precursors to macrophages, monocytes can be activated by R848, secreting several immune-promoting cytokines, such as IL-1, IL-6, IL-12 and TNF-α [66]. Macrophages and DCs also possess a high degree of phagocytic activity that can be leveraged in the context of drug delivery [67]. Cationic nanoparticles have been demonstrated to exhibit increased interaction with macrophages and DCs, and this likely explains the relatively high percentage of DiI+ DCs [68]. DCs are the most efficient APC, express a high level of TLR 7 and TLR 8, and help coordinate the innate and adaptive immunity by secreting inflammatory cytokines such as IFNs and TNF-α [32]. Lastly, we observed a relatively high level of DiI+ NK cells (roughly 8% of all DiI+ cells). NK cells express functional TLR 7 and TLR 8 and can be stimulated by R848. Stimulation of NK cells with R848 leads to upregulation of cell surface marker CD69 and increased cytotoxicity independent of accessory cells. R848 stimulation of NK cells also produces differential production of IFN-γ. The production of IFN-γ is dependent on the presence of co-stimulation of NK cells by IL-2 or IFN-α, secreted from accessory monocytes. Resting NK cells will not increase the production of IFN-γ to in response to R848, yet will secrete large amounts of IFN-γ in the presence of monocytes which have also been stimulated by R848 to release IL-2, IL-12 and IFN-α. NK cell secretion of IFN-γ is critical for the initiation of the innate immune response and promoting the T_{h1} immune response that is both anti-viral and anti-tumouricidal. The T_{h1} response can also favour the polarization of macrophages to an inflammatory M1-like phenotype and reduce levels of Tregs, MDSCs and TAMs which promote tumour immunosuppression. Therefore, secretion of cytokines such as TNF-α, IL-6 and IFN-α is highly desirable for activation of NK cells and overcoming tumour immunosuppression.

3.2 Aim 2: In vivo efficacy and mechanistic study of DSTAP-R848 relative to free R848 and vehicle control.

3.2.1 *In Vivo* Cytokine Induction by DSTAP-R848 and Free R848

The next sub-aim was to investigate the stimulation of immune cells in the peritoneal cavity by DSTAP-R848. We focused on investigating key cytokines that are known to be released from monocytes, macrophages and DCs after activation by TLR 7 and TLR 8 agonists [31], including IFN-α, IL-6 and TNF-α. Mice (BALB/C, female) were IP injected with PBS (negative control), free R848 or DSTAP-R848. At 15 min, 1 h, 4 h and 24 h, mice were scarified, and IP cell pellet was collected. After cell lysis, qPCR was used to determine the level of mRNA expression of the cytokines. As summarized in **Figure 10**, DSTAP-R848 increased the level of IFN-α mRNA in the IP cells by 5- and 2-fold compared to free drug at 4 and 24 h, respectively. DSTAP-R848 also increased IFN-α mRNA by 4-, 6- and 10-fold compared to PBS treatment at 1 h, 4 h, and 24 h, respectively. Conversely, free R848 only significantly upregulated IFN-α mRNA by 4-fold compared to PBS after long time exposure for 24 h, however there was no significant difference at 15 min, 1 h or 4 h post injection.

A similar trend was observed for IL-6 and TNF-α, although the effect was less pronounced. For both IL-6 and TNF-α, levels of mRNA expression were similar among the PBS, free R848 and DSTAP-R848 groups for the 15 min, 1 h and 4 h time points. However, at 24 h, IL-6 and TNF-α mRNA expression was increased by 2-fold in the DSTAP-R848 group relative to PBS ($p<0.005$), while free R848 failed to upregulate these two cytokines in the IP cells. Overall, DSTAP-R848 was able to significantly upregulate all three cytokines in the IP cells and the effect increased over a 24 h period; the effect was particularly strong for IFN-α.

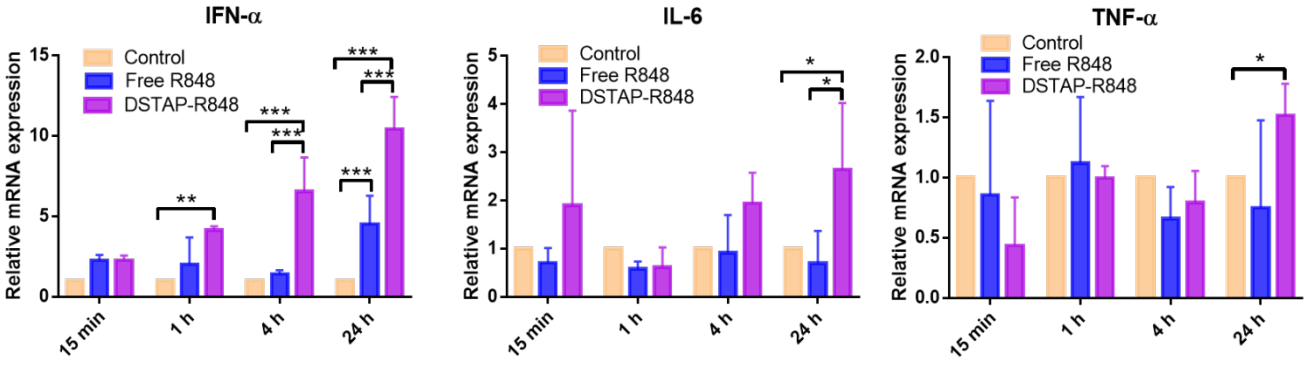

Figure 10. Expression levels of mRNA of IFN-α, IL-6 and TNF-α in IP cells after IP injection of PBS, Free R848 or DSTAP-R848 into BALB/C mice. Data = mean ±SD, n=5. * indicates $p<0.05$; *** indicates $p<0.001$.

Following the finding that DSTAP-R848 increased the mRNA expression of IFN-α, IL6 and TNFα in the IP cells with the most profound effect in IFN-α, we next sought to determine whether IFNα levels in the plasma and peritoneal fluid were also increased. We administered either free R848 or DSTAP-R848 via IP injection and then retrieved plasma and IP fluid samples over the course of 24 h. To measure the cytokine level, we used a sandwich ELISA. In the peritoneal fluid we observed that DSTAP-R848 treatment resulted in a significant 3-fold increase in IFN-α concentration relative to the free drug group at 1 h (70 vs 23 ng/mL). However, by 4 h, this effect had subsided without any significant difference (<5 ng/mL) and the IFN-α level was under the detection limit at 24 h. Conversely, there was no difference between the IFN-α level in the plasma between free R848 and DSTAP-R848 group, and both treatments induced a peak concentration of ~40 ng/mL at 1 h, followed by a rapid decline to <5 ng/mL at 4 h and then under the detection limit at 24 h. Notably, the IFN-α level in the peritoneal fluid (70 ng/mL) was higher than that in the plasma (40 ng/mL) for the DSTAP-R848 group, whereas the situation was reversed for the free drug group (23 ng/mL vs 38 ng/mL) (**Figure 11**). The cytokine results are consistent with the PK and BD data, showing increased retention of DSTAP-R848 compared to free R848 in the peritoneum

and comparable overall plasma exposure, which resulted in enhanced cytokine induction in the peritoneum but not in the plasma by DSTAP-R848.

We focused on examining IFN-α, which is the major cytokine induced by R848 and the key cytokine that can turn a "cold" tumour to "hot", leading to improved prognosis [69]. IFN-α is an immunomodulatory cytokine which belongs to the Type 1 Interferon family of signalling proteins and demonstrates anti-viral and anti-tumour properties. IFN-α is secreted by monocytes in response to stimulation by TLR 7 and TLR 8 agonists and serves to upregulate the expression of MHC-1 on DCs thereby increasing the presentation of antigen to helper T cells [70]. Increased antigen presentation activates the adaptive immune response and prime cytotoxic CD8+ T cells. In addition, IFN-α is a potent inducer of NK cell activity and upregulates their cytotoxicity both directly and by suppression of IL-12 secretion [71,72]. Overall, IFN-α serves to prime CD8+ T cells and upregulate the innate immune system through NK cells for antitumour activity.

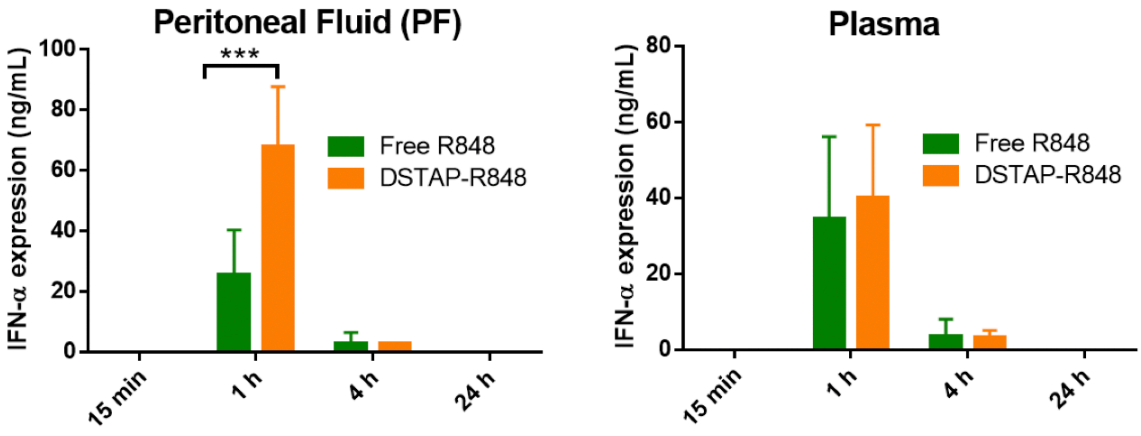

Figure 11. IFN-α levels in the peritoneal fluid and plasma after IP administration of free R848 and DSTAP-R848 in BALB/C mice. N=5, $p<0.005$.

3.2.2 Efficacy and Tolerability Study of DSTAP-R848 vs Free R848 in a Murine PC Model

Mice received an IP injection of $2x10^5$ CT-26-Luc cells/mouse on day -4, and then were administered IP OXA at 6 mg/kg on day 0, followed by an IP injection of PBS, free R848 or DSTAP-R848 on Day 1 at 8 mg R848/kg (**Figure 12A**). OXA is often included in standard chemotherapy for PC, and therefore, was incorporated in the treatment regimens. Tumour progression in the peritoneum was monitored and quantified by bioluminescence imaging. As shown in **Figure 12B**, mice treated with OXA alone displayed rapid tumour progression, while those treated with OXA + free R848 showed initial reduction in tumour growth on Day 3-4, but the tumours quickly regrew and spread on day 5-13. On day 13, there was no difference between the OXA alone and OXA + free R848 groups (**Figure 12C**). The initial inhibition of tumour progression in the OXA + free R848 group could be due to that free R848 induced IFN-α that exhibited significant antitumour effect. However, this combination did not induce prolonged antitumour efficacy, and the tumours returned rapidly. In contrast, OXA + DSTAP-R848 started showing antitumour efficacy on day 3 and the PC was consistently inhibited on day 3-13, and on day 13 the tumour load measured by bioluminescence was 3-fold significantly lower than the other two groups. The data suggest that OXA+ DSTAP-R848 induced prolonged antitumour immunity. We also compared the impact of the treatments on the health of mice using body weight as a proxy. Throughout the study there was no significant changes in the body weight averages of each group indicating the DSTAP-R848 did not cause increased toxicity at a cost of increased efficacy. However, on days 7-13 there was a downward trend in the body weight of the three groups where the PBS mice lost approximately 10% of the average body weight, Free R848 group lost ~5% body weight and the DSTAP-R848 group lost ~7%. (**Figure 12D**). In the PBS group, this could be due to tumour burden and subsequent cachexia. In the free R848 group we believe this may be due to hypophagia from R848 stimulation which has been documented in literature [73]. Finally, in the DSTAP-R848 group, this could be due to tumour burden loss as the imaging data indicate tumours shrank during this time frame in addition to hypophageia. This would account for the increased body weight loss relative to the free drug group.

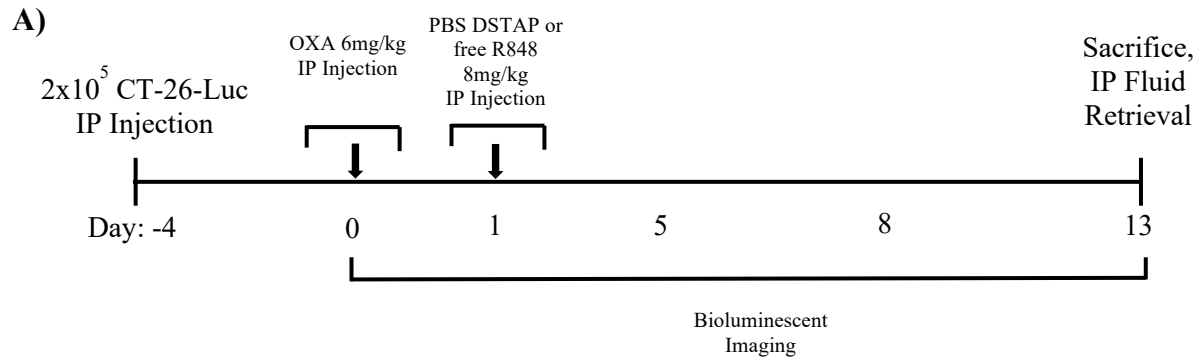
A)
2x10^5 CT-26-Luc
IP Injection
OXA 6mg/kg
IP Injection
PBS DSTAP or
free R848
8mg/kg
IP Injection
Sacrifice,
IP Fluid
Retrieval
Day: -4
0
1
5
8
13
Bioluminescent
Imaging

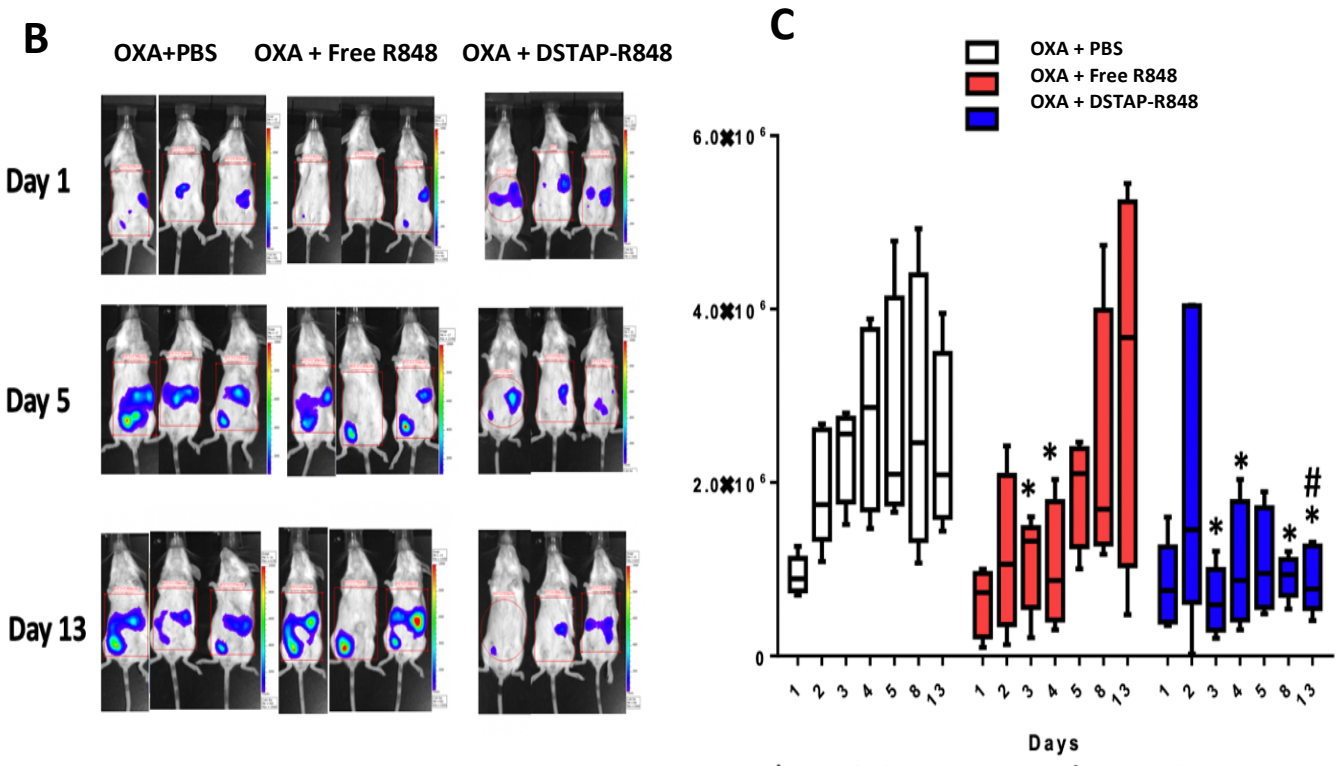
B
OXA+PBS
OXA + Free R848
OXA + DSTAP-R848
Day 1
Day 5
Day 13
C
OXA + PBS
OXA + Free R848
OXA + DSTAP-R848
6.0✖10^6
4.0✖10^6
2.0✖10^6
0
Days

D)

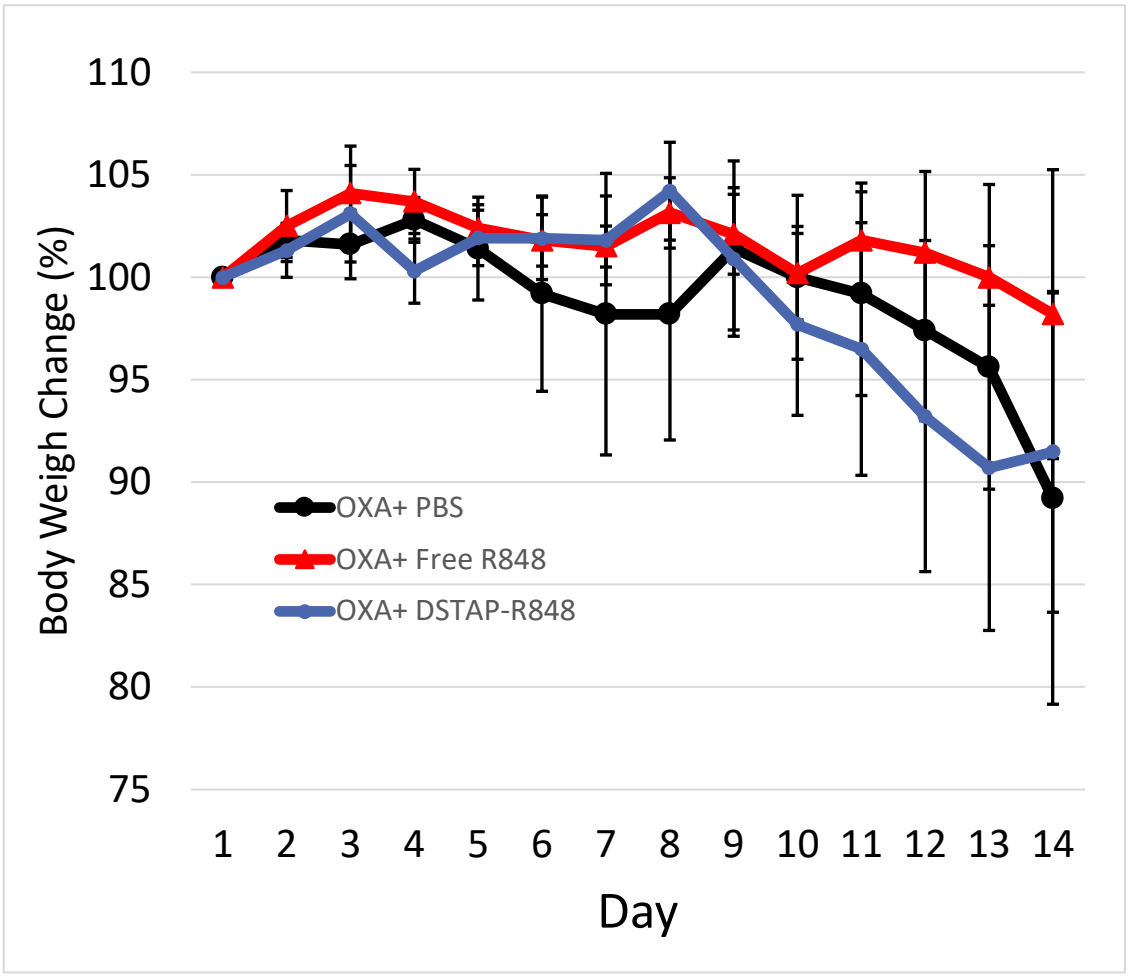

Figure 12. *In vivo* efficacy and tolerability studies against CT-26-Luc **A)** Treatment schedule diagram. **B)** Representative bioluminescent images of mice in different treatment arms. **C)** Graphical summary of semi-quantitative bioluminescent image data of CT-26-Luc tumours in mouse peritoneum plotted over the study duration. *= $p < 0.05$ relative to PBS and # = $p < 0.05$ relative to free R848. **D)** Body weight change of mice after different treatments (Data = mean, ± SD, n=5-6).

We were able to achieve a significant reduction in tumour burden by a single round of therapy at a relatively low concentration (8 mg/kg). Future studies could explore the possibility of repeat dosing to further boost immune potentiation in the peritoneal cavity. Evidence from Michaelis et al. 2019 [73]

suggests that the low dose infusion model of R848 is tolerable as indicated by their cachexia mouse model which investigated weight loss, sleep cycles and food intake in addition to muscle and fat wasting during pancreatic cancer and R848 treatment. This was in accordance with our studies that R848 in both free drug and DSTAP-liposome formulations was tolerable, and mice recovered over a 5-day period from initial weight loss.

3.2.3 Preliminary Investigation into How DSTAP-R848 Modulated the Peritoneal Immune Cell Composition

The efficacy data suggest OXA + DSTAP-R848 induced prolonged antitumour immunity. To test the proposed mechanism depicted in Figure 15, we examined the change in immune cell populations in the tumour microenvironment (i.e. peritoneal fluid) after different treatments (OXA only, OXA + free R848, OXA + DSTAP-R848). Mice were sacrificed on day 10, and the cells collected from the IP fluid were stained using fluorescent antibodies and analyzed by fluorescence activated cell sorting (FACS). The gating strategy for our FACS analysis is outlined in **Figure 13A**. In preliminary initial studies, we noticed no significant differences in B and T cell levels, so they were not measured in this study, however, this study is planned to be re-investigated using new antibodies (see Chapter 5 for future plans). In the FACS study outlined below, we observed that the DSTAP-R848 treated mice demonstrated increased levels of NK cells (Nkp46+), **(Figure 13 B, C**), however, this result represents only an initial result as more mice are required to confirm this finding and generate significance. In regard to DCs, there were no observable differences in CD80 expression levels. CD80 is often expressed early in DC activation and thus, this may represent activation by tumour inoculation reflected in all treatment groups [34]. The late activation marker CD86 was not able to be quantified as the antibody failed to generate any response. We plan to re-investigate both markers in a future study described below in Chapter 5.

A)

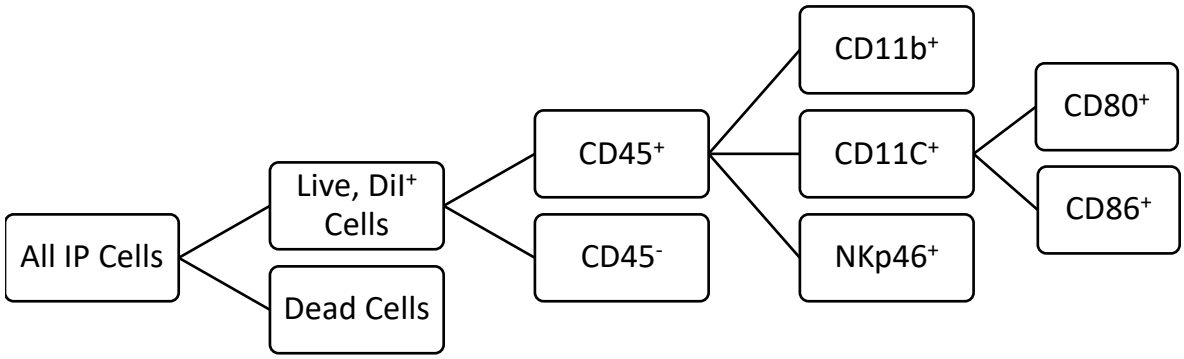
All IP Cells
Live, DiI+ Cells
Dead Cells
CD45+
CD45-
CD11b+
CD11C+
NKp46+
CD80+
CD86+

B)

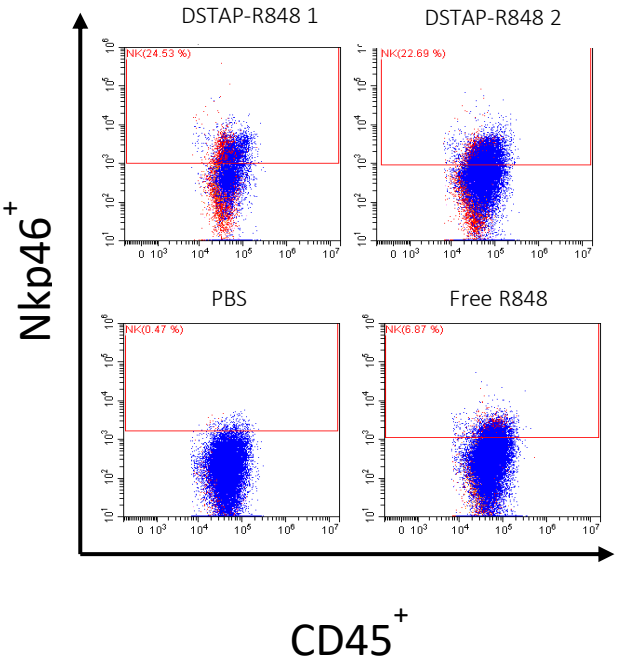
DSTAP-R848 1
DSTAP-R848 2
PBS
Free R848
NK(24.53 %)
NK(22.69 %)
NK(0.47 %)
NK(6.87 %)
NKp46+
CD45+

C)

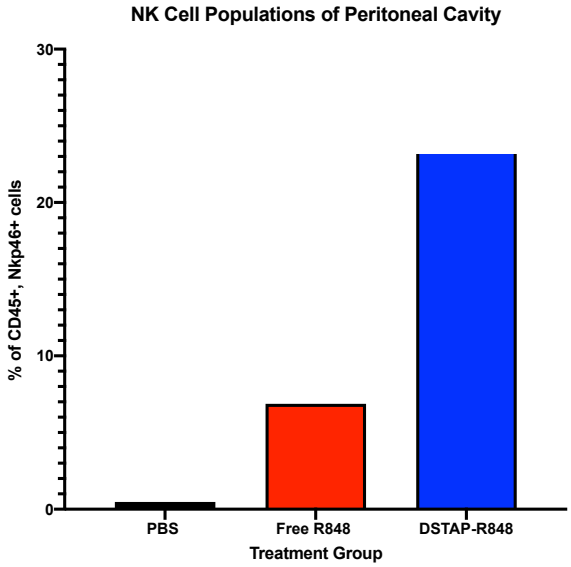
NK Cell Populations of Peritoneal Cavity
% of CD45+, Nkp46+ cells
30
20
10
0
PBS
Free R848
DSTAP-R848
Treatment Group

D)

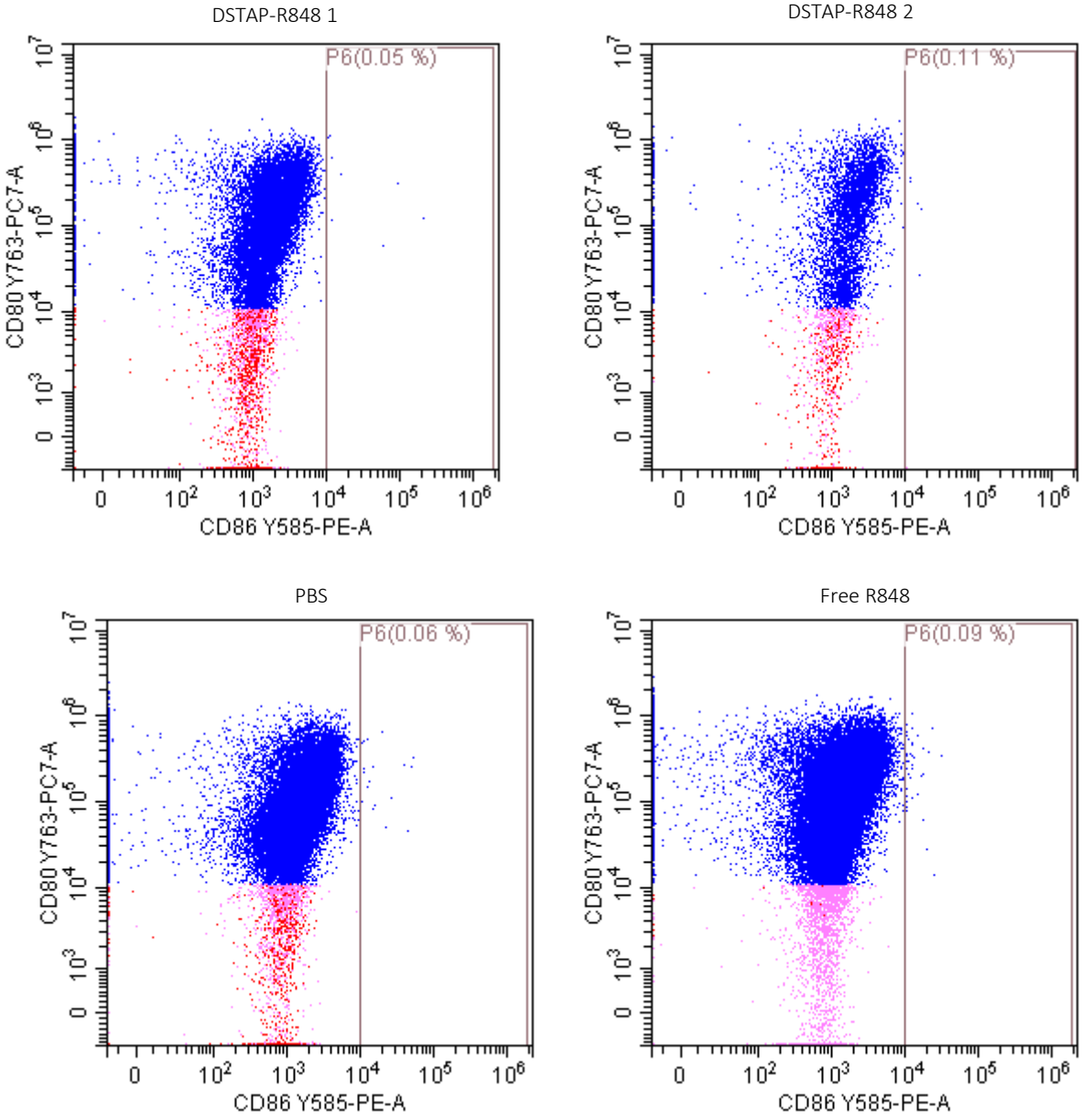

Figure 13. FACS analysis of immune cell composition in the peritoneal fluid after different treatments. **A)** Schematic of the gating strategy used in FACS analysis. **B)** Representative flow cytometer images gated based on CD45+, NKp46+ to present NK cell populations from 4 mice (2 DSTAP treated, 1 free R848 treated and 1 PBs treated) gated to show NK cell populations. **C)** Populations of NK cells represented graphically (n=1-2). D) Representative flow cytometer images gated

based on CD45+ CD11C+, CD80+ CD86+ to present activation of DC cell populations from 4 mice (2 DSTAP treated, 1 free R848 treated and 1 PBs treated)

The finding of elevated NK cell populations in the DSTAP-R848 group is well supported by our other studies and the past literature findings investigating NK cell influx into the peritoneal cavity from immunostimulatory compounds [51]. After stimulation by R848, monocytes secrete IL-12 and colony stimulating factor, which contribute to NK cell expansion. R848 also can act directly on NK cells and induce the secretion of large quantities of type I IFNs and TNF-α and increase NK cytotoxicity to tumours [74,75]. Despite characterizing a variety of cells in this study, there remains several questions to be answered. Importantly, we did not observe differences in levels of CD8 T cells, yet OXA + DSTAP-R848 appeared to induce antitumour immunity. Second, TLR 7 stimulation by R848 is known to expand B cell populations both directly and by TLR7 and TLR 8 mediated release of IFN-α and IL-6 from associated cells such as fibroblasts, and monocytes [76]. In our study we did not observe an increase in B cell populations in the peritoneal cavity although this was likely due to the short time frame. B cell proliferation requires up to 10 days after stimulation from cytokines such as IL-6 and thus would not be detected in our assay [66,77]. It is possible these cells were increased but a time point we did not measure. In regard to T cells, it is possible that similar to B cells, T cells were increased in the PF but at an earlier time point. Alternatively, DSTAP-R848 could have acted by increasing tumour infiltration of CD8+ T cells. Either possibility implores further investigation into the mechanisms behind the observed antitumour efficacy (see Chapter 5).

Chapter 4: Summary

Peritoneal cancer is often characterized by aggressive spreading in the abdominal cavity and enclosed organs. PC has remained difficult to treat owing to its diffuse spreading and strong immunosuppressive activity; both these attributes contribute to high rates of recurrence. We hypothesized

that PC therapy would benefit from a targeted liposomal immunotherapeutic approach to boost anti-tumour immunity and reduce tumor burden

After compiling the data from the immune cell uptake, cytokine stimulation, and finally the efficacy data, and framing this into the reference of current literature, we propose a mechanism for the efficacy of the combination therapy of OXA + DSTAP-R848. In this model, OXA serves to induce immunogenic cell death leading to the release of tumour associated antigens (TAAs). TAAs are subsequently phagocytosed by APCs such as monocytes and DCs and upon stimulation by DSTAP-R848 will upregulate the presentation of TAAs on MHC-II and secrete cytokines such as IFN-α, TNF-α and IL-6. These cytokines, likely in conjugation with others, cause the expansion of NK cells and upregulate the priming of CD4+ T cells and activation of CD8+ T cells. These cytotoxic T lymphocytes induce TAA-specific tumour lysis, which in turn produces more TAAs to further promote antitumour immunity (**Figure 14**).

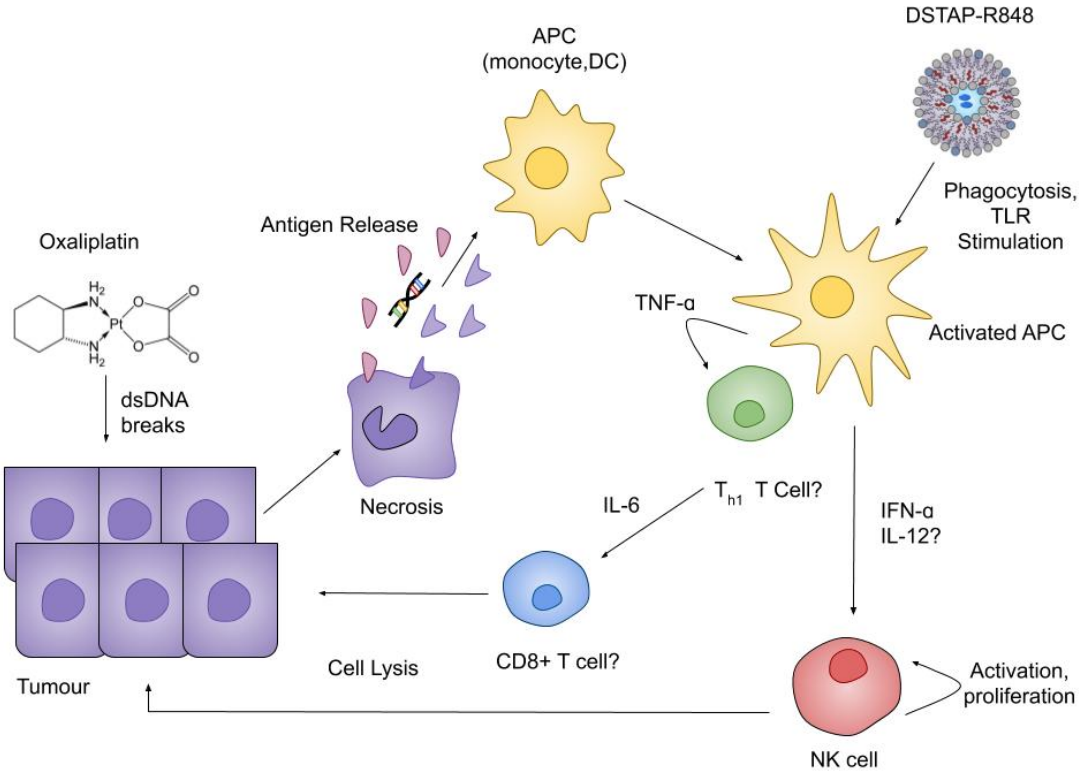

Figure 14. Proposed antitumour mechanism of OXA + DSTAP-R848.

4.1 Aim 1: Liposome Characterization, PK/BD of DSTAP-R848 and Cellular Distribution

We first demonstrated that cationic DSTAP-liposomes displayed increased peritoneal retention compared to its anionic and neutral counterparts, and the DSTAP-liposomes were efficiently internalized by cells, accumulating in the endosomes where TLR7 and TLR 8 reside. We then formulated R848 into the DSTAP-liposomes and discovered that DSTAP-R848 displayed increased peritoneal retention after IP administration compared to free R848; the peritoneal fluid-to-plasma ratio of R848 was increased by 15 times in the DSTAP-R848 group relative to free R848. Additionally, while DSTAP-R848 was effectively taken up by the IP immune cells, no drug could be recovered in the IP cells from the free R848 group. Among the IP cells that took up the DSTAP-liposomes, 50%, 10%, and 8% of them were monocytes, DCs, and NK cells, respectively.

4.2 Aim 2: Efficacy, tolerability and modulation of immune cell composition

The DSTAP-R848 group demonstrated a significant increase in the mRNA expression of inflammatory cytokines, including TNF-α (2-fold), IL-6 (2.5-fold) and IFN-α (10-fold) relative to control. Furthermore, the DSTAP-R848 mice demonstrated 3-fold increased IFN-α level in the peritoneal fluid relative to the free drug, while there was no significant difference in the plasma IFN-α levels, suggesting selective immune stimulating in the peritoneum by DSTAP-R848.

In combination with OXA, DSTAP-R848 effectively suppressed tumour growth in an aggressive PC model in mice. At the study endpoint, mice treated with OXA + DSTAP-R848 displayed 3-fold reduced tumour load compared to those treated with OXA alone, or OXA + free R848. In a preliminary study, we observed elevated NK cell levels in the peritoneal fluid of DSTAP-R848 treated mice compared to the other groups.

Chapter 5: Future Plans

To further examine the mechanism of this combination therapy, we must to perform more in-depth studies. We need to examine the immune cell composition in the peritoneum microenvironment by including new markers for a broader range of immune cells including macrophages (Ly6G/C or GR-1), T cells (CD3, CD4, CD8), and re-examine the DC activation through new CD80/86 antibodies. This should provide a more complete picture of the change in immune cell composition after OXA + DSTAP-R848 treatment. We also plan to examine tumour nodules from each group and characterize the immune cell infiltration. The data will be compared with that obtained from the peritoneal fluid. We plan to investigate the presence of T_{reg} cells, myeloid derived suppressor cells, tumour associated macrophages (TAMS) (M2-like), NK cells and CD8+ T cells in the tumour. In addition, we hope to examine biomarkers of immunosuppression such as PDL1 and CTLA-4. We hypothesize that tumours in the DSTAP-R848 will show increases in CD8+:CD4+ T cell ratio and reduced expression of inhibitory cell surface markers such as PDL-1 and CTLA-4. We also hypothesize DSTAP-R848 will reduce levels of M2 like macrophages and polarize TAMS to M1-like states. To facilitate this, we have retrieved tumours from the efficacy study and had begun to cryosection them to stain with fluorescent antibodies. We will also perform tumour digests and FACS to further analyse the immune cells infiltrating in the tumour.

To investigate whether OXA + DSTAP-R848 promotes long term and specific antitumour immunity, we will perform a splenocyte activation study. In brief, splenocytes will be collected from mice on day 7, and incubated with medium isolated from cultured CT-26-Luc cells that undergo ICD by hyperthermia. The splenocytes will then be analyzed for intracellular level of IFN-γ by FACS. If an antigen-specific antitumour immunity is developed, the intracellular level of IFN-γ in T cells will be elevated upon exposure to the antigen.

Finally, a future experiment will further investigate the mechanisms of immune cell mediated tumour clearance by IP injection of immune cell depleting antibodies. In this study, antibodies against different CTLs will be used to determine the impact of these cells in tumour clearance.

Despite R848 being shown to be tolerable in a topical formulation as indicated by FDA approval more extensive studies are required to demonstrate its safety in animal models when administered in liposomal formulation. More in depth and long-term studies will be required to determine if repeat dosing also is safe in animals and can be measured using the correlates of weight loss, sleep and eating cycles, biochemical analysis of serum and IP fluid proteins, cytokine and chemokine levels and finally histopathological analysis of organs. If the formulation is deemed safe and effective in animals, we believe that the DSTAP-liposomal formulation could serve as a new first-in-class adjuvant to the traditional chemotherapeutic regime for PC, generating longer and more robust remission.

References

[1] A. Isaza-Restrepo, J.S. Martin-Saavedra, J.L. Velez-Leal, F. Vargas-Barato, R. Riveros-Dueñas, The peritoneum: Beyond the tissue - A review, Front. Physiol. 9 (2018) 1–12. https://doi.org/10.3389/fphys.2018.00738.

[2] Z. Lu, J. Wang, M.G. Wientjes, J.L.S. Au, Intraperitoneal therapy for peritoneal cancer, Futur. Oncol. 6 (2010) 1625–1641. https://doi.org/10.2217/fon.10.100.

[3] Y. Yonemura, E. Canbay, Y. Endou, H. Ishibashi, A. Mizumoto, M. Miura, Y. Li, Y. Liu, K. Takeshita, M. Ichinose, N. Takao, M. Hirano, S. Sako, G. Tsukiyama, Peritoneal cancer treatment, Expert Opin. Pharmacother. 15 (2014) 623–636. https://doi.org/10.1517/14656566.2014.879571.

[4] P.E. Bonnot, G. Piessen, V. Kepenekian, E. Decullier, M. Pocard, B. Meunier, J.M. Bereder, K. Abboud, F. Marchal, F. Quenet, D. Goere, S. Msika, C. Arvieux, N. Pirro, R. Wernert, P. Rat, J. Gagnière, J.H. Lefevre, T. Courvoisier, R. Kianmanesh, D. Vaudoyer, M. Rivoire, P. Meeus, G. Passot, O. Glehen, J. Abba, M. Alyami, N. Bakrin, J.L. Bernard, F. Bibeau, D. Bouzard, C. Brigand, S. Carrère, M. Carretier, B. Castel, E. Cotte, B. Celerier, C. Ceribelli, C. De Chaisemartin, V. De Franco, S. Deguelte-Lardiere, J.R. Delpero, G. Desolneux, F. Dumont, C. Eveno, S. Durand-Fontanier, S. Evrard, O. Facy, F.N. Gilly, P. Gourdiole, J.M. Guilloit, B. Heyd, B. Lelong, R. Lo Dico, V. Loi, P. Mariani, J.L. Meffert, P. Ortega-Deballon, B. Paquette, C. Petorin, P. Peyrat, D. Pezet, J.M. Regimbeau, S. Rohr, C. Sabbagh, J.F. Seitz, O. Sgarbura, I. Sielezneff, I. Sourrouille, A. Taibi, E. Thibaudeau, J.J. Tuech, J. Vanbockstael, F. Zinzindohoue, Cytoreductive Surgery with or without Hyperthermic Intraperitoneal Chemotherapy for Gastric Cancer with Peritoneal Metastases (CYTO-CHIP study): A propensity score analysis, J. Clin. Oncol. 37 (2019) 2028–2040. https://doi.org/10.1200/JCO.18.01688.

[5] M. Gelli, J.F.L. Huguenin, T. de Baere, L. Benhaim, A. Mariani, V. Boige, D. Malka, I. Sourouille, M. Ducreux, D. Elias, D. Goéré, Peritoneal and extraperitoneal relapse after previous curative treatment of peritoneal metastases from colorectal cancer: What survival can we expect?, Eur. J. Cancer. 100 (2018) 94–103. https://doi.org/10.1016/j.ejca.2018.04.015.

[6] J.J. Skitzki, E.A. Repasky, S.S. Evans, Hyperthermia as an immunotherapy strategy for cancer, Curr. Opin. Investig. Drugs. 10 (2009) 550–558.

[7] V.J. Verwaal, H. Van Tinteren, S. V. Ruth, F.A.N. Zoetmulder, Toxicity of Cytoreductive Surgery and Hyperthermic Intra-Peritoneal Chemotherapy, J. Surg. Oncol. (2004). https://doi.org/10.1002/jso.20013.

[8] C.T. Seebauer, S. Brunner, G. Glockzin, P. Piso, P. Ruemmele, H.J. Schlitt, E.K. Geissler, S. Fichtner-Feigl, R. Kesselring, Peritoneal carcinomatosis of colorectal cancer is characterized by structural and functional reorganization of the tumor microenvironment inducing senescence and proliferation arrest in cancer cells, Oncoimmunology. 5 (2016) 1–12. https://doi.org/10.1080/2162402X.2016.1242543.

[9] E. Halkia, J. Spiliotis, P. Sugarbaker, Diagnosis and management of peritoneal metastases from ovarian cancer, Gastroenterol. Res. Pract. 2012 (2012). https://doi.org/10.1155/2012/541842.

[10] C.S. Chu, A.W. Menzin, D.G.B. Leonard, S.C. Rubin, J.E. Wheeler, Primary Peritoneal Carcinoma: A Review of the Literature, Obstet. Gynecol. Surv. 54 (1999). https://journals.lww.com/obgynsurvey/Fulltext/1999/05000/Primary_Peritoneal_Carcinom

a__A_Review_of_the.23.aspx.
[11] M. Wang, J. Zhao, L. Zhang, F. Wei, Y. Lian, Y. Wu, Z. Gong, S. Zhang, J. Zhou, K. Cao, X. Li, W. Xiong, G. Li, Z. Zeng, C. Guo, Role of tumor microenvironment in tumorigenesis, J. Cancer. (2017). https://doi.org/10.7150/jca.17648.
[12] V. Chew, H.C. Toh, J.P. Abastado, Immune microenvironment in tumor progression: Characteristics and challenges for therapy, J. Oncol. (2012). https://doi.org/10.1155/2012/608406.
[13] D.A. Leinster, H. Kulbe, G. Everitt, R. Thompson, M. Perretti, F.N.E. Gavins, D. Cooper, D. Gould, D.P. Ennis, M. Lockley, I.A. McNeish, S. Nourshargh, F.R. Balkwill, The peritoneal tumour microenvironment of high-grade serous ovarian cancer, J. Pathol. 227 (2012) 136–145. https://doi.org/10.1002/path.4002.
[14] M. Binnewies, E.W. Roberts, K. Kersten, V. Chan, D.F. Fearon, M. Merad, L.M. Coussens, D.I. Gabrilovich, S. Ostrand-Rosenberg, C.C. Hedrick, R.H. Vonderheide, M.J. Pittet, R.K. Jain, W. Zou, T.K. Howcroft, E.C. Woodhouse, R.A. Weinberg, M.F. Krummel, Understanding the tumor immune microenvironment (TIME) for effective therapy, Nat. Med. 24 (2018) 541–550. https://doi.org/10.1038/s41591-018-0014-x.
[15] E.L.J.M. Smits, P. Ponsaerts, Z.N. Berneman, V.F.I. Van Tendeloo, The Use of TLR7 and TLR8 Ligands for the Enhancement of Cancer Immunotherapy, Oncologist. (2008). https://doi.org/10.1634/theoncologist.2008-0097.
[16] N.M. Luheshi, J. Coates-Ulrichsen, J. Harper, S. Mullins, M.G. Sulikowski, P. Martin, L. Brown, A. Lewis, G. Davies, M. Morrow, R.W. Wilkinson, Transformation of the tumour microenvironment by a CD40 agonist antibody correlates with improved responses to PD-L1 blockade in a mouse orthotopic pancreatic tumour model, Oncotarget. (2016). https://doi.org/10.18632/oncotarget.7610.
[17] Q.V. Le, J. Choi, Y.K. Oh, Nano delivery systems and cancer immunotherapy, J. Pharm. Investig. 48 (2018) 527–539. https://doi.org/10.1007/s40005-018-0399-z.
[18] M.W.L. Teng, M.H. Kershaw, M.J. Smyth, Cancer Immunoediting: From Surveillance to Escape, Cancer Immunother. Immune Suppr. Tumor Growth Second Ed. 3 (2013) 85–99. https://doi.org/10.1016/B978-0-12-394296-8.00007-5.
[19] S. Yang, H. Gao, Nanoparticles for modulating tumor microenvironment to improve drug delivery and tumor therapy, Pharmacol. Res. 126 (2017) 97–108. https://doi.org/10.1016/j.phrs.2017.05.004.
[20] G. Kroemer, L. Galluzzi, O. Kepp, L. Zitvogel, Immunogenic Cell Death in Cancer Therapy, Annu. Rev. Immunol. (2013). https://doi.org/10.1146/annurev-immunol-032712-100008.
[21] K. Wang, T. Shen, G.P. Siegal, S. Wei, The CD4/CD8 ratio of tumor-infiltrating lymphocytes at the tumor-host interface has prognostic value in triple-negative breast cancer, Hum. Pathol. 69 (2017) 110–117. https://doi.org/10.1016/j.humpath.2017.09.012.
[22] T.F. Gajewski, H. Schreiber, Y.X. Fu, Innate and adaptive immune cells in the tumor microenvironment, Nat. Immunol. 14 (2013) 1014–1022. https://doi.org/10.1038/ni.2703.
[23] R.H. Farnsworth, M. Lackmann, M.G. Achen, S.A. Stacker, Vascular remodeling in cancer, Oncogene. 33 (2014) 3496–3505. https://doi.org/10.1038/onc.2013.304.
[24] M.A. Swartz, A.W. Lund, Lymphatic and interstitial flow in the tumour microenvironment: Linking mechanobiology with immunity, Nat. Rev. Cancer. 12 (2012) 210–219. https://doi.org/10.1038/nrc3186.
[25] A. Rotte, Combination of CTLA-4 and PD-1 blockers for treatment of cancer, J. Exp.

Clin. Cancer Res. (2019). https://doi.org/10.1186/s13046-019-1259-z.
[26] D.R. Parkinson, Present status of biological response modifiers in cancer, Am. J. Med. 99 (1995) 54s-56s. https://doi.org/10.1016/S0002-9343(99)80288-5.
[27] P. Christmas, Toll-Like Receptors: Sensors that Detect Infection, Nat. Educ. (2010).
[28] S. Adams, Toll-like receptor agonists in cancer therapy, Immunotherapy. (2009). https://doi.org/10.2217/imt.09.70.
[29] S. Kaczanowska, A.M. Joseph, E. Davila, TLR agonists: our best frenemy in cancer immunotherapy , J. Leukoc. Biol. (2013). https://doi.org/10.1189/jlb.1012501.
[30] H. Hemmi, T. Kaisho, O. Takeuchi, S. Sato, H. Sanjo, K. Hoshino, T. Horiuchi, H. Tomizawa, K. Takeda, S. Akira, Small-antiviral compounds activate immune cells via the TLR7 MyD88-dependent signaling pathway, Nat. Immunol. 3 (2002) 196–200. https://doi.org/10.1038/ni758.
[31] D.H. Dockrell, Imiquimod and resiquimod as novel immunomodulators, J. Antimicrob. Chemother. (2001). https://doi.org/10.1093/jac/48.6.751.
[32] M.A. Stanley, Imiquimod and the imidazoquinolones: Mechanism of action and therapeutic potential, Clin. Exp. Dermatol. 27 (2002) 571–577. https://doi.org/10.1046/j.1365-2230.2002.01151.x.
[33] H. Tanji, U. Ohto, T. Shibata, K. Miyake, T. Shimizu, Structural reorganization of the toll-like receptor 8 dimer induced by agonistic ligands, Science (80-.). (2013). https://doi.org/10.1126/science.1229159.
[34] M.M. Alam, D. Yang, A. Trivett, T.J. Meyer, J.J. Oppenheim, HMGN1 and R848 Synergistically Activate Dendritic Cells Using Multiple Signaling Pathways, Front. Immunol. (2018). https://doi.org/10.3389/fimmu.2018.02982.
[35] T. Spinetti, L. Spagnuolo, I. Mottas, C. Secondini, M. Treinies, C. Rüegg, C. Hotz, C. Bourquin, TLR7-based cancer immunotherapy decreases intratumoral myeloid-derived suppressor cells and blocks their immunosuppressive function, Oncoimmunology. (2016). https://doi.org/10.1080/2162402X.2016.1230578.
[36] C.B. Rodell, S.P. Arlauckas, M.F. Cuccarese, C.S. Garris, R. Li, M.S. Ahmed, R.H. Kohler, M.J. Pittet, R. Weissleder, TLR7/8-agonist-loaded nanoparticles promote the polarization of tumour-associated macrophages to enhance cancer immunotherapy, Nat. Biomed. Eng. (2018). https://doi.org/10.1038/s41551-018-0236-8.
[37] S.R. Mullins, J.P. Vasilakos, K. Deschler, I. Grigsby, P. Gillis, J. John, M.J. Elder, J. Swales, E. Timosenko, Z. Cooper, S.J. Dovedi, A.J. Leishman, N. Luheshi, J. Elvecrog, A. Tilahun, R. Goodwin, R. Herbst, M.A. Tomai, R.W. Wilkinson, Intratumoral immunotherapy with TLR7/8 agonist MEDI9197 modulates the tumor microenvironment leading to enhanced activity when combined with other immunotherapies, J. Immunother. Cancer. (2019). https://doi.org/10.1186/s40425-019-0724-8.
[38] P.M. Chen, W.Y. Pan, C.Y. Wu, C.Y. Yeh, C. Korupalli, P.K. Luo, C.J. Chou, W.T. Chia, H.W. Sung, Modulation of tumor microenvironment using a TLR-7/8 agonist-loaded nanoparticle system that exerts low-temperature hyperthermia and immunotherapy for in situ cancer vaccination, Biomaterials. (2020). https://doi.org/10.1016/j.biomaterials.2019.119629.
[39] P.J. Tacken, I.S. Zeelenberg, L.J. Cruz, M.A. Van Hout-Kuijer, G. Van De Glind, R.G. Fokkink, A.J.A. Lambeck, C.G. Figdor, Targeted delivery of TLR ligands to human and mouse dendritic cells strongly enhances adjuvanticity, Blood. 118 (2011) 6836–6844. https://doi.org/10.1182/blood-2011-07-367615.

[40] G. Pauli, W.-L. Tang, S.-D. Li, Development and Characterization of the Solvent-Assisted Active Loading Technology (SALT) for Liposomal Loading of Poorly Water-Soluble Compounds, Pharmaceutics. 11 (2019) 465. https://doi.org/10.3390/pharmaceutics11090465.
[41] M.J. Ernsting, M. Murakami, A. Roy, S.D. Li, Factors controlling the pharmacokinetics, biodistribution and intratumoral penetration of nanoparticles, J. Control. Release. (2013). https://doi.org/10.1016/j.jconrel.2013.09.013.
[42] M.L. Briuglia, C. Rotella, A. McFarlane, D.A. Lamprou, Influence of cholesterol on liposome stability and on in vitro drug release, Drug Deliv. Transl. Res. 5 (2015) 231–242. https://doi.org/10.1007/s13346-015-0220-8.
[43] L. Galluzzi, A. Buqué, O. Kepp, L. Zitvogel, G. Kroemer, Immunogenic cell death in cancer and infectious disease, Nat. Rev. Immunol. (2017). https://doi.org/10.1038/nri.2016.107.
[44] A. Serrano-del Valle, A. Anel, J. Naval, I. Marzo, Immunogenic cell death and immunotherapy of multiple myeloma, Front. Cell Dev. Biol. (2019). https://doi.org/10.3389/fcell.2019.00050.
[45] A.M. Abel, C. Yang, M.S. Thakar, S. Malarkannan, Natural killer cells: Development, maturation, and clinical utilization, Front. Immunol. (2018). https://doi.org/10.3389/fimmu.2018.01869.
[46] J.C. Sun, J.N. Beilke, L.L. Lanier, Adaptive immune features of natural killer cells, Nature. (2009). https://doi.org/10.1038/nature07665.
[47] A. Glasner, A. Levi, J. Enk, B. Isaacson, S. Viukov, S. Orlanski, A. Scope, T. Neuman, C.D. Enk, J.H. Hanna, V. Sexl, S. Jonjic, B. Seliger, L. Zitvogel, O. Mandelboim, NKp46 Receptor-Mediated Interferon-γ Production by Natural Killer Cells Increases Fibronectin 1 to Alter Tumor Architecture and Control Metastasis, Immunity. (2018). https://doi.org/10.1016/j.immuni.2017.12.007.
[48] U. Hadad, T.J. Thauland, O.M. Martinez, M.J. Butte, A. Porgador, S.M. Krams, NKp46 clusters at the immune synapse and regulates NK cell polarization, Front. Immunol. (2015). https://doi.org/10.3389/fimmu.2015.00495.
[49] D.H. Raulet, R.E. Vance, Self-tolerance of natural killer cells, Nat. Rev. Immunol. (2006). https://doi.org/10.1038/nri1863.
[50] S. Paul, G. Lal, The molecular mechanism of natural killer cells function and its importance in cancer immunotherapy, Front. Immunol. (2017). https://doi.org/10.3389/fimmu.2017.01124.
[51] P. Marconi, F. Bistoni, A. Cassone, L. Frati, M. Baccarini, E. Garaci, E. Bonmassar, The role of the peritoneal cavity in successful treatment of a murine lymphoma with chemotherapy and non-specific immunostimulation, Cancer Immunol. Immunother. (1982). https://doi.org/10.1007/BF00205313.
[52] M. Cheng, Y. Chen, W. Xiao, R. Sun, Z. Tian, NK cell-based immunotherapy for malignant diseases, Cell. Mol. Immunol. (2013). https://doi.org/10.1038/cmi.2013.10.
[53] C. Guillerey, N.D. Huntington, M.J. Smyth, Targeting natural killer cells in cancer immunotherapy, Nat. Immunol. (2016). https://doi.org/10.1038/ni.3518.
[54] S. Dadashzadeh, N. Mirahmadi, M.H. Babaei, A.M. Vali, Peritoneal retention of liposomes: Effects of lipid composition, PEG coating and liposome charge, J. Control. Release. (2010). https://doi.org/10.1016/j.jconrel.2010.08.026.
[55] W.L. Tang, W.H. Tang, A. Szeitz, J. Kulkarni, P. Cullis, S.D. Li, Systemic study of

solvent-assisted active loading of gambogic acid into liposomes and its formulation optimization for improved delivery, Biomaterials. 166 (2018) 13–26. https://doi.org/10.1016/j.biomaterials.2018.03.004.
[56] C.U. Nd, S.U. Mma, Resiquimod Compound Summary, 2020.
[57] S. Shaker, A. Gardouh, M. Ghorab, Factors affecting liposomes particle size prepared by ethanol injection method, Res. Pharm. Sci. (2017). https://doi.org/10.4103/1735-5362.213979.
[58] A.L. Engel, G.E. Holt, H. Lu, The pharmacokinetics of Toll-like receptor agonists and the impact on the immune system, Expert Rev. Clin. Pharmacol. (2011). https://doi.org/10.1586/ecp.11.5.
[59] D.J. Dowling, Recent Advances in the Discovery and Delivery of TLR7/8 Agonists as Vaccine Adjuvants, ImmunoHorizons. 2 (2018) 185–197. https://doi.org/10.4049/immunohorizons.1700063.
[60] A. Ray, B.N. Dittel, Isolation of mouse peritoneal cavity cells, J. Vis. Exp. (2010). https://doi.org/10.3791/1488.
[61] T.J. Mercolino, L.W. Arnold, L.A. Hawkins, G. Haughton, Normal mouse peritoneum contains a large population of Ly-l+ (CD5) B cells that recognize phosphatidyl choline: Relationship to cells that secrete hemolytic antibody specific for autologous erythrocytes, J. Exp. Med. (1988). https://doi.org/10.1084/jem.168.2.687.
[62] A.A. Cassado, M.R. D'Império Lima, K.R. Bortoluci, Revisiting mouse peritoneal macrophages: Heterogeneity, development, and function, Front. Immunol. (2015). https://doi.org/10.3389/fimmu.2015.00225.
[63] J.C. Ochando, C. Homma, Y. Yang, A. Hidalgo, A. Garin, F. Tacke, V. Angeli, Y. Li, P. Boros, Y. Ding, R. Jessberger, G. Trinchieri, S.A. Lira, G.J. Randolph, J.S. Bromberg, Alloantigen-presenting plasmacytoid dendritic cells mediate tolerance to vascularized grafts, Nat. Immunol. (2006). https://doi.org/10.1038/ni1333.
[64] L. Vidard, M. Kovacsovics-Bankowski, S.K. Kraeft, L.B. Chen, B. Benacerraf, K.L. Rock, Analysis of MHC class II presentation of particulate antigens by B lymphocytes, J. Immunol. (1996).
[65] J. Li, D.R. Barreda, Y.A. Zhang, H. Boshra, A.E. Gelman, S. LaPatra, L. Tort, J.O. Sunyer, B lymphocytes from early vertebrates have potent phagocytic and microbicidal abilities, Nat. Immunol. (2006). https://doi.org/10.1038/ni1389.
[66] A.T. Bender, E. Tzvetkov, A. Pereira, Y. Wu, S. Kasar, M.M. Przetak, J. Vlach, T.B. Niewold, M.A. Jensen, S.L. Okitsu, TLR7 and TLR8 Differentially Activate the IRF and NF-κB Pathways in Specific Cell Types to Promote Inflammation, ImmunoHorizons. (2020). https://doi.org/10.4049/immunohorizons.2000002.
[67] P.J. Leenen, K. Radosević, J.S. Voerman, B. Salomon, N. van Rooijen, D. Klatzmann, W. van Ewijk, Heterogeneity of mouse spleen dendritic cells: in vivo phagocytic activity, expression of macrophage markers, and subpopulation turnover., J. Immunol. (1998).
[68] S. Kumar, A.C. Anselmo, A. Banerjee, M. Zakrewsky, S. Mitragotri, Shape and size-dependent immune response to antigen-carrying nanoparticles, J. Control. Release. 220 (2015) 141–148. https://doi.org/10.1016/j.jconrel.2015.09.069.
[69] Q. Duan, H. Zhang, J. Zheng, L. Zhang, Turning Cold into Hot: Firing up the Tumor Microenvironment, Trends in Cancer. (2020). https://doi.org/10.1016/j.trecan.2020.02.022.
[70] S. Gessani, L. Conti, M. Del Cornò, F. Belardelli, Type I interferons as regulators of

human antigen presenting cell functions, Toxins (Basel). (2014). https://doi.org/10.3390/toxins6061696.
[71] C.A. Biron, K.B. Nguyen, G.C. Pien, L.P. Cousens, T.P. Salazar-Mather, NATURAL KILLER CELLS IN ANTIVIRAL DEFENSE: Function and Regulation by Innate Cytokines, Annu. Rev. Immunol. (1999). https://doi.org/10.1146/annurev.immunol.17.1.189.
[72] C.A. Biron, Role of early cytokines, including alpha and beta interferons (IFN-α/β), in innate and adaptive immune responses to viral infections, Semin. Immunol. (1998). https://doi.org/10.1006/smim.1998.0138.
[73] K.A. Michaelis, M.A. Norgard, X. Zhu, P.R. Levasseur, S. Sivagnanam, S.M. Liudahl, K.G. Burfeind, B. Olson, K.R. Pelz, D.M. Angeles Ramos, H.C. Maurer, K.P. Olive, L.M. Coussens, T.K. Morgan, D.L. Marks, The TLR7/8 agonist R848 remodels tumor and host responses to promote survival in pancreatic cancer, Nat. Commun. 10 (2019) 1–15. https://doi.org/10.1038/s41467-019-12657-w.
[74] Y.T. Bryceson, S.C.C. Chiang, S. Darmanin, C. Fauriat, H. Schlums, J. Theorell, S.M. Wood, Molecular mechanisms of natural killer cell activation, J. Innate Immun. (2011). https://doi.org/10.1159/000325265.
[75] O.M. Hart, V. Athie-Morales, G.M. O'Connor, C.M. Gardiner, TLR7/8-Mediated Activation of Human NK Cells Results in Accessory Cell-Dependent IFN-γ Production, J. Immunol. 175 (2005) 1636–1642. https://doi.org/10.4049/jimmunol.175.3.1636.
[76] M.I. Vazquez, J. Catalan-Dibene, A. Zlotnik, B cells responses and cytokine production are regulated by their immune microenvironment, Cytokine. (2015). https://doi.org/10.1016/j.cyto.2015.02.007.
[77] M.H. Soesatyo, Janeway's Immunobiology, J. Teknosains. (2012). https://doi.org/10.22146/teknosains.5992.